Fouling composition during membrane treatment of secondary effluent: microscale characterization leading to fouling prevention on the pilot scale

National Water Research Institute
and
Orange County Water District

Principal Investigator: Harry Ridgway
Co-Principal Investigator: Greg Leslie

Grisel G. Rodriguez
Don W. Phipps

Water Resources and Technology Department
Orange County Water District
P.O. Box 8300
10500 Ellis Ave.
Fountain Valley, CA 927288-8300

April 30, 2001

TABLE OF CONTENTS

INTRODUCTION

State -of-the-art pressure driven membrane separation technologies have emerged in recent years as essential elements of modern water and wastewater treatment practice. Membrane separation processes are typically efficient and economical; however, they are also highly susceptible to surface fouling problems, including the unwanted accumulation of bacteria and other microorganisms (or microbial products) on the membrane surfaces (biofouling). Biofouling results from (i) initial attachment of bacteria to the membrane surface (stemming from the inherent cell-membrane affinity), (ii) pressure driven accumulation resulting from the transmembrane flux and other hydrodynamic properties of the system, (iii) growth and multiplication of the attached population at the expense of feedwater nutrients, and (iv) physical entrainment within an existing biofilm. Microbial growth in a surface biofilm is typically associated with the elaboration of extracellular polymeric substances (EPS), often acidic heteropolysaccharides and/or glycoproteins, that help stabilize cellular attachment and offer protection from biocidal agents or other adverse conditions (e.g., drying). The EPS exhibits the properties of a hydrated gel (hydrogel), thereby functioning as a diffusional barrier to water and solutes. It also prevents surface cross-flow that normally prevents formation of ion polarization. The diffusion limitation appears to be largely responsible for the observed decline in water flux and solute rejection in those membrane systems that have become severely biologically fouled.

The microscale structure of biofilms play a critical role in determining the ability of nutrients, biocides, cleaning agents, and other substances to penetrate to critical sites within the biofilm matrix. Some recently developed analytical techniques should provide a significant advance to our current primitive understanding of membrane biofouling processes and identify novel and effective anti-biofouling strategies.

Microscope flow cells (MFCs) of various design configurations have been developed to allow direct microscopic visualization and quantification of attached biofilm cells under dynamic flow conditions (4, 16, 25). The MFCs may be used exclusively in the

laboratory to grow and observe axenic or native mixed species biofilms under controlled physicochemical and hydrodynamic conditions or they may be placed on-line in an actual membrane facility to monitor biofilm formation from designated feedwaters. In membrane biofouling studies, MFCs may be used to explore and identify (at the microscopic scale) physical or chemical conditions which disrupt biofilms (e.g., new chemical cleaning agents) or that interfere with or otherwise influence biofilm growth kinetics (e.g., biocides). The MFC should be sufficiently flexible in design to accommodate different flow channel geometries (e.g., channel depth and length). Poor MFC design or machining invariably results in flow cells that leak or that are cumbersome and time consuming to use on a routine basis.

The application of confocal scanning laser microscopy (CSLM) to biofilm research has provided detailed 3D information on the structural complexity of fully hydrated living biofilms (26), and also, a non-invasive tool to study the biofilms (22). We relied on deconvolution algorithms to reconstruct 3-D images from stacks of optical sections, rather than using conventional confocal microscopy because this method was faster, letting us acquire single images in as little as a few nanoseconds, and additionally reduced vibration artifacts and fluorochrome fading. The digital deconvolution microscope and 3D imaging system could be organized into modules that were combined in varying ways depending on the specific imaging task.

Bright-field microscopy and differential interference contrast (DIC) microscopy are minimally invasive techniques for investigating deposition and growth of bacteria, or the removal of bacteria by cleaning agents. In this case, differential interference contrast is the most useful technique. Since bright illumination tends to impede bacterial growth, very low white-light illumination, filtered to remove the IR components, is used to image the growing biofilms.

Two- and three-dimensional fluorescent techniques are used to locate specific features within a biofilm. Various fluorochromes can be used to localize individual cells within the biofilm or to assess the nature of cell physiology.

The current investigation seeked to apply these methods to address specific questions concerning the earliest stages of membrane biofouling, including initial cell attachment. Furthermore, these methods are being applied to identify and evaluate the antibiofouling action of a wide range of chemical agents and to learn how these agents work on a submicron or molecular level. This report summarizes the major highlights of this research.

MATERIALS AND METHODS

Deconvolution fluorescence microscopy for observation and analysis of membrane biofilms. A unique microscope system that permits both two-dimensional (2D) and three-dimensional (3D) viewing of membrane biofilms from any desired perspective is schematically outlined in Figure 1 and depicted in Figure 2. This system combines advanced optical microscope imaging and deconvolution techniques recently reviewed by Shaw and Phipps et al. (19 and 21) with robotic sampling and digital image processing methods to create virtual models of microbial biofilms on water processing membranes. Several 3D image stacks may be acquired under different imaging (filtration) conditions and combined to produce a color-coded volume that simultaneously maps multiple biofilm features (e.g., dual or triple dye staining). The resulting models may be used to investigate specific biofilm features such as the distribution of specific microorganisms and extracellular polysaccharides, the nature of biofilm fluid channels, or the penetration of biocides or other molecules into the biofilm matrix.

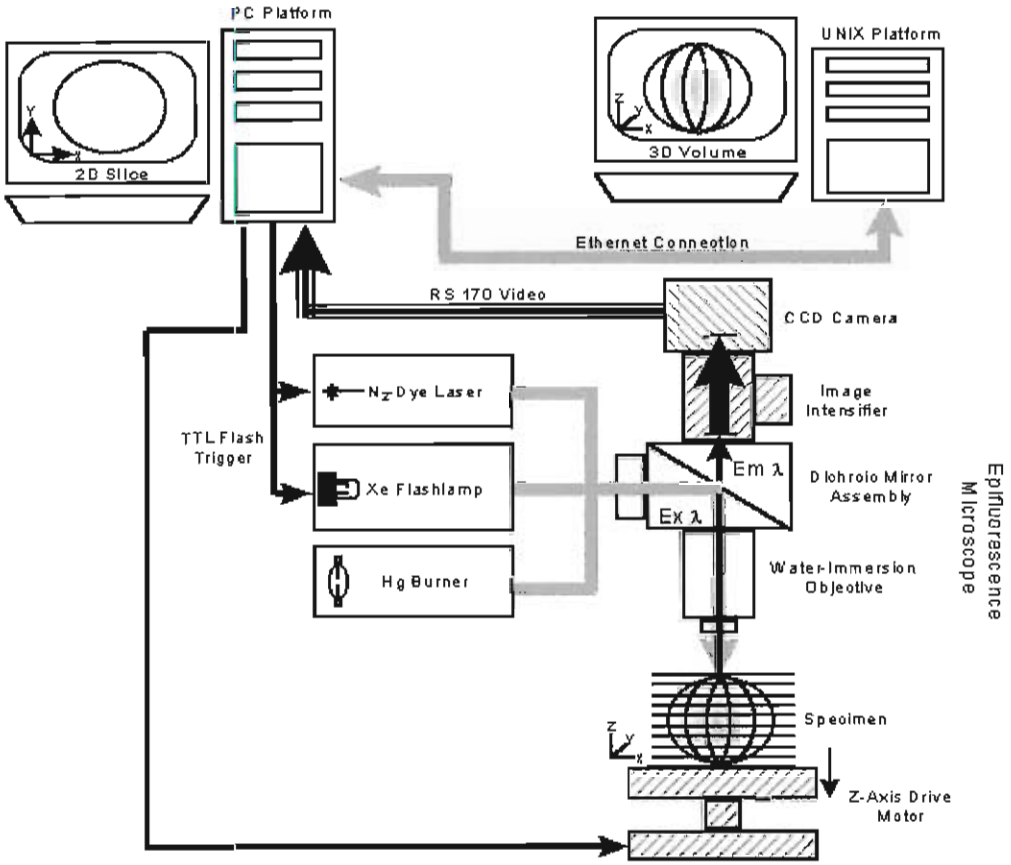

Figure 1. Schematic of digital deconvolution microscope and 3D imaging system for investigating membrane biofilm structure. The PC platform coordinates the cooled camera, xenon flash/N-laser systems, and automated (z-axis) stage mechanism to collect 2D image stacks. Basic 2D image processing operations include background correction, deconvolution, and contrast/brightness adjustments. UNIX platform combines 2D image stacks into 3D volumes. Volume processing operations include 3D viewing of 1-3 overlaid volumes, volume color assignments and false color rendering, morphometric measurements and volume dissections, and movie loop productions. See text for details.

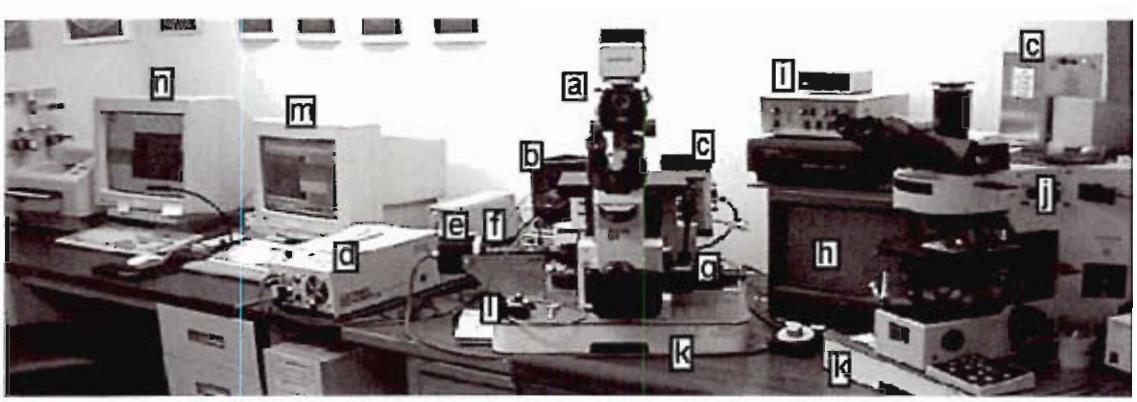

Figure 2. Main components of digital deconvolution microscope system: inverted microscope (a), mercury burner (b), xenon flash unit (c), nitrogen laser-pumped pulsed dye laser with optical fiber couplings (d), cooled CCD camera (e), image intensifier (f), Ludl z-axis stage drive mechanism (g), live image monitor (h), video intensity analyzer (i), upright microscope system (j), vibration dampening tables (k), gain control for intensifier (l), PC platform for 2D image capture, image manipulation, and z-axis sectioning control (m), and UNIX platform for 3D volume reconstruction, volume morphometry, and dissections (n). See text for details.

Epifluorescence light microscopes and objectives. Biofilm specimens were imaged using either an Olympus IX-70 inverted microscope or an Olympus AX-70 upright microscope. These microscopes feature infinity-corrected optics and were each equipped with three epifluorescent filter cubes; a wide UV (U-MWU, excitation 330-385 nanometers (nm), dichroic cutoff=400 nm, emission >420nm), a wide blue (U-MWB, excitation 450-480 nm, dichroic cutoff=500 nm, emission >515 nm), and a wide green (U-MWG, excitation 510-550 nm, dichroic cutoff=570 nm, emission >590 nm). The microscopes and filter cubes are stock configurations and readily available from Olympus (Olympus America, Inc., Melville, NY). Both microscopes were also equipped with a UPlanApo 60x 1.2 NA W PSF objective (Olympus). This special water immersion objective is corrected for coverglass thickness and designed to produce nearly aberration-free images over its entire working distance through aqueous media. It is suitable for work with thin window flow cells (see below). In addition, planapochromatic 40x air and 100x oil immersion UV-transmission objectives were also occasionally employed (Olympus).

Fluorescence excitation sources. One of two discontinuous (flash) sources were typically utilized for imaging. The first source was a 2600 series EG&G flashlamp kit modified to fit an Olympus microscope condenser lamp housing and equipped with a FX-249-U short-arc xenon flashlamp (EG&G Electro-Optics, Salem, MA). This system provides a broadband source of white light when driven with 1 joule of electrical energy per pulse. Manufacturer's specifications indicate that the overall flash duration from this source is 100 μsec; however, peak illumination intensity occurs at 15 μsec and the majority of the energy is emitted between 10 and 30 μsec. Overall light energy output is rated at 1000-2000 μjoules/pulse emitted over a spectral range from 280 to 1100nm. Because high-pressure xenon arcs emit almost continuous spectra from 300 to 800nm, the excitation properties of this source are essentially that of the particular filter cube being used. The flash energy was collimated and directed into the microscope using a quartz condenser assembly (Opti Quip, Highland Mills, NY).

The second excitation system consisted of a nitrogen laser-pumped dye laser (Oriel model 79111 low pressure N_2 laser pumping an Oriel model 79120 dye laser module,

Oriel Instruments, Stratford, CT). This system was used to provide a source of monochromatic pulsed light for fluorochrome excitation. Either the 337 nm nitrogen laser line or the tunable dye laser output (350-750 nm +/- 0.4 nm) was directed into the microscope via a 1000 μm diameter single quartz fiber optic and quartz microscope coupler (Laser Sciences, Inc., Franklin, MA). Laser transmission through such large single fibers is characterized by uneven light output as a result of constructive and destructive interference between the fiber's multiple transmission modes. Transmission mode "scrambling" was achieved by providing two sharp bends in the fiber using a small pair of clamps set at right angles to each other near the microscope adapter. This treatment produced an evenly illuminated circular output beam of monochromatic light from the fiber. The nitrogen laser pump produced >300 μjoules/pulse with a flash duration of 5 ns. Dye laser energy output varied depending on the coupling efficiency of the dye, but according to the manufacturer, output should range from about 25 to 63 μjoules/pulse at 4 ns/pulse. Dyes for laser operation are obtained premixed from Laser Science, Inc., Franklin, MA. Laser excitation with the UV filter cube was achieved by either using the nitrogen laser output directly or by using the dye laser with BBQ (4,4'''-bis[(2-butyloctyl)oxy]-1,1':4',1'':4'',1'''-quaterphenyl, 1mM in *p*-dioxane; lasing range: 380 to 395 nm). Excitation with the blue and green filter cubes was achieved using Coumarin 500 (7-(ethylamino)-4-(trifluoromethyl)-2H-1-benzopyran-2-one, 9.33 mM in methanol; lasing range: 485 to 570 nm). Dyes have stored in the dark at room temperature in completely filled and sealed individual 1x1cm quartz cuvettes. A magnetic "flea" stir bar in the cuvettes driven during laser operation by a magnetic stirrer mounted below the cuvette holder provided sufficient dye circulation for stable laser output. Attenuation of laser excitation energy was accomplished when desired by tuning the dye laser toward the upper or lower pass band limits of the particular filter cube in use.

The above discontinuous excitation sources allow extremely rapid μs to ns image acquisition. Thus, the specimen was exposed to excitation radiation for the minimum time required to obtain an image. Therefore, fluorochrome fading was minimized without resorting to adulteration of the biofilm with antioxidant compounds. In addition, the extreme speeds of exposure rendered image acquisition nearly insensitive to

vibration error so that vibration isolation of the microscope was unnecessary. It is indeed possible to obtain 2D images of highly mobile specimens using these flash sources, such as bacteria carried with the bulk flow in a flow cell.

The stock 100 W mercury lamp provided with the Olympus microscopes produces continuous wave (CW) excitation, and this source was used when fluorochrome fading was not significant, when it was desirable to make visual observations of the specimen to quickly check results of a labeling protocol or to aid in locating an area of interest (AOI). A 3-way mirror housing (Opti Quip, Highland Mills, NY) fitted on each microscope allowed selection of any one of the three excitation sources prior to imaging.

Image acquisition. Microscope adjustments were made to properly accommodate the particular fluorochrome being imaged (choice of filter cube, light source, etc.). The biofilm specimen, either contained in a flow cell (see below) or prepared on a coverglass or coupon, was placed under the microscope and the fluorescence emission image from the specimen detected and amplified using a modified (manual gain control added) 3rd generation microchannel plate-type image intensifier providing 46 line pairs/mm spatial resolution and a maximum of 30,000x luminous gain (B. E. Meyers, Redmond, WA). The resulting intensified image was recorded with a cooled (-30C below ambient) optically-coupled HyperHAD 1/2 inch interline transfer charge coupled device (CCD) video camera (Dage IFG-300, Dage MTI, Inc., Michigan City, IN) acquiring at standard video frame rate (30 frames/second). Resulting images were inspected in real time with an in-line video monitor (Sony Trinitron PVM-1342Q, Sony Corp.). Real-time image intensity histogram data were visualized during image optimization procedures using an on-screen display analyzer (RasterScope, Dage MTI, Inc.).

Optimization of the camera and intensifier was accomplished by first setting the camera gain to maximum (+12dB gain) and, with the intensifier off, increasing the camera black level to eliminate dark noise. Following this, the image intensifier was activated and the intensifier gain increased to achieve video signal saturation of the brightest image

highlights. This method produced a well-contrasted image providing the full video signal range; however, adjustment of the camera black level and the intensifier gain beyond this point was sometimes required for badly contrasted specimens. In addition, when the laser excitation source was used, the laser excitation wavelength was also adjusted in coordination with the intensifier gain to provide the highest image contrast.

Image digitization and flash control. The resultant analog (RS 170) video signal from the camera was digitized to 640x480 rectangular pixels at 8 bits (256 gray levels) using a 266 Mhz PC-clone platform equipped with a FlashPoint 128 framegrabber (Integral Technologies, Indianapolis, IN). This board includes an output trigger and hardware/firmware to allow the use of a flash source to illuminate a video image. The board achieves flash synchronization using the video vertical sync portion of the RS-170 signal, and a user-selectable field delay allows time for the camera to process its illuminated fields before frame grabbing occurs (typically a three field delay was sufficient). Both flash sources require a TTL trigger signal (5 μsec square wave pulse, 3 to 5 volts) which was provided by connecting a 3 volt battery source in series with the closure switch output trigger of the framegrabber board. Programming allowed continuous display of images for composition at 2 to 3 frames/second; in addition, the laser provided an integral 30 Hz pulse generator that was used for real-time image visualization. Captured images were saved in standard tagged image file format (TIFF).

Calibration of 2D image X-Y axes. Pixel dimensions (dx and dy) of the 2D images were determined, for a given optical configuration, by imaging an optical micrometer consisting of precise parallel rulings spaced at 10 μm intervals (Bausch and Lomb, Rochester, NY). Measuring the number of pixels corresponding to the distance between the maximum number of lines across the field of view allowed accurate calculation of the μm/pixel ratio. The micrometer was mounted in water with a 0.170 micron thick (#1) coverglass placed over it and was imaged using brightfield (transmission) microscopy with water in the path between the objective and the coverglass to simulate specimen mounting conditions. This procedure was performed with the micrometer rulings in both vertical (to determine dx) and horizontal (to determine dy) orientations.

Volume sampling. A 3D "volume" of the biofilm specimen was sampled by obtaining a stack of 2D x-y plane "optical slices". Typically, ten images were averaged with the PC platform into each optical slice using Image-Pro Plus image processing software (Media Cybernetics, Silver Spring, MD) to compensate for intensity variations encountered with the flash excitation sources. The sequential optical slices (typically 50 to 170) were collected along the Z-axis by controlled movements of the microscope stage using a geared stepper motor system connected to the microscope fine focus control (Ludl MAC 2000 system, Ludl Electronic Products, Ltd., Hawthorne, NY) under the direction of software designed to coordinate image acquisition with stage movements (VolumeScan, VayTek, Inc., Fairfield, IA). The distance between slices (dz) chosen was typically a multiple of the optical slice pixel dimensions (dx, dy), usually 1:1 or 2:1. A dz of 0.3 to 0.6 μm was used during slice acquisition if the dx, dy of the slice was 0.3 μm, for example. Specimens were sampled from the bottom up due to requirements of the 3D reconstruction software. The use of custom macro programs greatly simplified volume acquisition and processing. Oversampling (obtaining slices spaced less than the depth of field of the objective and thus duplicating some of the information in the images) was desirable because it insured full representation of data along the Z-axis during 3D reconstruction, and increased Z-axis resolution. The time required for acquisition of a volume varied as a function of the number of optical slices in the volume and the number of images per slice. Collection of a volume composed of 100 slices with 10 images per slice required approximately 5 minutes.

Volumes were inspected along the Z-axis using a "top view" program that overlaid all the optical sections of the volume and projected their brightest pixels (maximum point projection) into the resultant composite image (VayTek, Inc., Fairfield, IA). This method was useful as a quality control step before more extensive image processing was attempted. Dimensions of sampled volumes varied depending on microscope optics used, but with the Olympus 60x PSF water immersion objective they typically ranged from 97-145 μm in the X-axis, 72-109 μm in the Y-axis, and 16-45 μm in the Z-axis (for 150 slices).

Volume pre-processing. All 2D image processing was carried out using Image-Pro Plus image processing software (Media Cybernetics, Silver Spring, MD). This package possesses a complete set of image processing tools, and in addition uses a rich macro language that allows the user to combine and automate all the tools into a broad spectrum of image processing filters. The background of uniformly recurring noise (defects in the image intensifier or camera, dust flecks on the optics, etc.) was eliminated from the volume by a user-defined macro that performed a running two-slice average over the entire volume to detect and then subtract the noise image from each slice in the volume. The processed volume thus contained only non-uniformly repeating information (e.g., the specimen). Image quality of all volume slices was enhanced when required by adjustment of the brightness, contrast and gamma settings (BCG) using functions provided by the image processing package combined in another user-defined macro. Results were checked over the entire volume by examining a top view.

Digital deconvolution of the volume. Defocused information (haze) was eliminated from each slice in the volume using a nearest-neighbor deconvolution algorithm in accordance with methods suggested by the manufacturer (MicroTome AT, VayTek, Inc., Fairfield, IA) based on the objective's theoretical point-spread function (PSF). Haze removal was typically set >90% and the dz value used for determination of the PSF was sometimes varied from the actual dz to obtain best results. It was, in most cases, possible to render focused objects in the fluorescent images (typically consisting of bright bacteria scattered in a dark background) with confocal quality, so that only objects in the depth of field of the objective remained in the slice (see Figure 3). Thus, following deconvolution, the "focused" volume contained little or no out of focus haze; just the focused information remained. The quality of the deconvolution was monitored both by checking selected individual slices and by rendering the deconvolved volume with a top view as previously described. Processing time on a 266 MHz PC averaged about 10 seconds/slice.

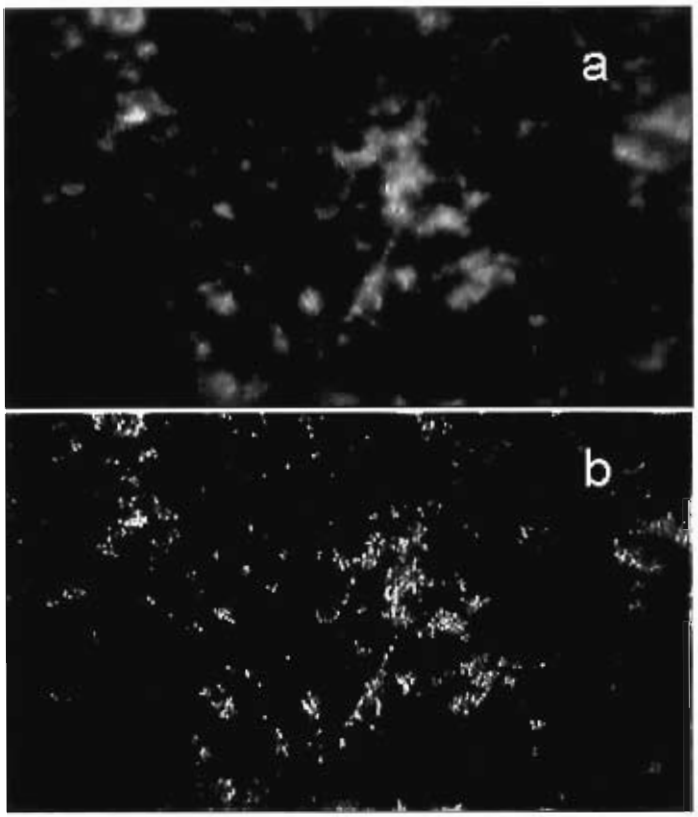

Figure 3. Raw (a) and digitally deconvolved image (b) of one optical section (thickness=0.3μ) of a wastewater biofilm on a CA-coated coverglass coupon. The 48-hour old biofilm was formed in a special microscope flow cell. Biofilm cells were stained with 0.1 μg/mL propidium iodide.

Volume post-processing. BCG adjustment was occasionally required to enhance the appearance of slices in the focused volume. In addition, the deconvolution algorithm occasionally enhanced very minute differences in the intensity of pixels comprising the odd and even video fields when using flash illumination, resulting in subtle one-pixel-wide horizontal "stripes" over the entire image. In this case, use of a macro that first applied a fast Fourier transform (FFT) to each slice, then excised the frequency component corresponding to the horizontal noise stripes and finally inverted the FFT to reconstitute the remaining image data effectively eliminated this artifact. In addition to these filters, volume slices were treated with other image filters (convolution algorithms such as sharpening, edge detection or enhancement algorithms, histogram optimization algorithms, etc.) as required to enhance features of interest prior to 3D rendering.

3D rendering of the volume. Volume slices were exported via an Ethernet link to a UNIX workstation (SGI Indigo Elan 4000, Silicon Graphics, Inc., Irvine, CA). A 3D rendering package (VoxBlast, VayTek, Inc., Fairfield, IA) used the 2D X-Y axis information (pixels) present in the optical slices and, based on the spacing between the slices and an interpolation algorithm, constructed a virtual model of the biofilm specimen made up of regular image cubes (voxels). Thus, all of the primary intensity and position data of objects in the original biofilm were represented in the rendered volume. The volume was rendered in low resolution (one out of three voxels rendered) to speed image processing while setting the 3D view angle, but palette and transparency (alpha channel) adjustments were made from highest resolution (every voxel) renderings to provide complete data for analysis and recording.

The volume required trimming to remove thin "dead" regions at its extreme X and Y faces. False coloring of gray values was achieved using a user-defined palette map, and colors were chosen to enhance features of interest in the rendered volume. Where required, two palettes were applied to halves of the volume to help reveal internal details masked by structures of low transparency. Lighting models were also occasionally applied to enhance the 3D effect and emphasize opaque features (such as bacteria). A polygon rendering feature allowed multiple, color-coded polygon overlays to be applied to the volume. This overlay feature was typically used to outline the outer dimensions of the volume to aid visual orientation during volume rotation and display.

Calibration of the 3D volume Z-axis. Accurate spatial rendering of the volume along the Z-axis was achieved by calibration of the 3D rendering software with targets of known Z-axis geometry. Fluorescent latex spheres with diameters ranging from 0.5 to 6.0 μm (Fluoresbrite Calibration Grade Size Range Kit, Polysciences, Inc., Warrington, PA) embedded in a gel matrix of distilled water solidified with 0.7% purified agar (Becton Dickinson Microbiological Systems, Cockeysville, MD) were used for this purpose. Stocks produced by mixing beads of specific diameters with the melted agar in 24 ml scintillation vials were prepared in advance and stored at 4°C until use. Bead specimens were prepared by melting a bead/agar stock in a microwave oven, then placing a drop of the melted mixture on a glass slide at room temperature and

immediately dropping a cover glass on top of the drop. The agar quickly solidified and immobilized the beads, creating a sample over 100 μm thick containing evenly distributed fluorescent targets of defined geometry.

The bead target slide was sampled as described above and reconstructed in 3D. The shape of the beads was examined in a top-view of the volume to confirm dx/dy accuracy, then examined along the X-Y plane (perpendicular to the optical slice plane), where the rendering software entirely synthesizes the view. The magnitude of deviation from a spherical appearance of the beads was determined throughout the length of the Z-axis. The software interslice distance was adjusted until the interpolation algorithm properly rendered the beads as spheres. The degree of this adjustment was typically very minor for the 60x water immersion objective, which is specifically engineered not to introduce significant spherical aberration with deep specimens. Volumes in excess of 40 μm thickness were reconstructed with little or no required correction. However, volumes sampled using the more common (and far less expensive) oil immersion or air objectives produce significant compression or elongation artifacts when viewed along the X-Y plane. Alteration of the interslice distance using the bead targets as a guide allowed limited compensation of these distortions, and accurate 3D reproduction was in fact possible with these more common microscope objectives so long as the biofilm specimen thickness did not exceed 5 μm or so and was not viewed through an excessive depth of media (it was possible to accurately render a thin biofilm on the inner surface of a flow cell window, for instance).

Processing of the rendered volume. It was possible to examine the rendered image volume from any desired orientation. In addition, two dimensional (2D) slice planes could be passed through the volume either parallel to the original slice planes or at random orientations within the volume, and the resulting view extracted to a 2D image for examination. An independent color palette was assigned to this extracted image to emphasize elements of interest not obvious within the original 3D volume. In addition, resampling along an axis perpendicular to the random slice plane allowed extraction of all or part of the original volume into a volume with a user-defined orientation, such as down the axis of a biofilm channel.

Measurements performed on the rendered volume included morphometric determinations in 3D and 2D (including biofilm thickness, distances between biofilm bacteria or microcolonies, and dimensions of biofilm channels). Analysis of gray level distributions allowed relative determination of fluorochrome concentrations in both 2D and 3D.

Views of the rendered volume were extracted and saved as 24 bit RGB TIFF images. A movie loop generator was used to produce rotating views of the volume, providing up to 360 degrees of rotation in either altitude or azimuth (individually or simultaneously). This technique provides a smooth rotation of the rendered biofilm specimen and presents a view from all sides which often aids visualization of biofilm details hidden behind the specimen. In addition, by producing a full rotation using 120 frames, 60 stereo pairs (3 degree tilt) result that represent the biofilm from all visual aspects of its rotation.

Combination of multiple volumes for multifluorochrome imaging. Biofilms stained with multiple fluorochromes (up to three) were sequentially sampled under conditions designed to detect each of the fluorochromes in turn. The resulting volumes were saved separately (a macro has been designed for this purpose) and processed independently using the methods described above. Each volume was then imported into the rendering software as either the "red", "green", or "blue" channel and a composite renderer was used to produce a colored volume in which all the features of the component volumes were displayed simultaneously. This allowed the spatial distribution of bacteria (imaged using generic nuclear stains) in the biofilms to be directly compared with the location of polysaccharides (e.g., detected using calcofluor white). Special considerations when performing this type of imaging must be given to the intensity histograms of each of the volumes; the gray level distributions should be matched as well as possible to maximize the final image dynamic range (intensifier gain for each volume must be adjusted independently due to differences in the sensitivity of the intensifier at different wavelengths and possibly the effects of different excitation sources if more than one is used).

Preparation and casting of cellulose acetate (CA) thin films on microscope coverglasses. It was often useful to prepare defined model membrane surfaces that could be used to investigate bacterial adsorption and desorption phenomena by direct microscopic methods (see below). In this case, there is a requirement that the membrane polymer be cast onto the surface of a suitable inert carrier or support material such as glass. Certain polymer systems, e.g., CA homopolymers or heteropolymer blends of CA comprising different degrees of acetylation, are especially well suited for this purpose since they can be prepared as monophasic solutions which can be readily cast onto inert glass or metal support materials. The CA-coated coverglasses created in this manner can then be incorporated into special flow cells (see below) which permit the measurement of bacterial adsorption/desorption kinetics. Polymers of CA (approximately 100,000 MW) with varying levels of acetylation (~40 wt% - 43.9 wt% acetyl content) were obtained from Eastman Kodak, Inc., Rochester, NY. The CA polymers were dissolved (at 0.5 wt%) in high purity dichloromethane (B&JGC, Burdick & Jackson, Muskegon, MI). Solutions were mixed with a Teflon® stir bar and sonicated in a warm water bath (50-60^{O}C) until the CA completely dissolved. Solutions were filtered through lens paper to remove insoluble fibrous material (i.e., undissolved CA). A Pyrex cylinder (20 x 6 cm O.D.) was used in the coating process (Figure 4). Compressed air passed through a dryer (Balston Model 75-20) and 0.2 μm polytetrafluoroethylene filter was used to continuously purge the cylinder of water vapor. Mixing of the CA solution was achieved with a Teflon® stir bar; however, both stirring and air purge were stopped just prior to casting of the CA film to eliminate turbulence at the air-solution interface which would result in uneven deposition of polymer. The coverglasses were secured to a fine copper wire with Teflon® adhesive tape and the wire attached to 2 lb test Nylon monofilament line with a brass swivel. Then, the line was tied to the drive shaft of a peristaltic pump (Masterflex, Cole-Parmer Instrument Co.). The coverglasses were dipped and withdrawn from the CA solution via the pump shaft rotation, providing a drawing rate of 1 cm/sec. The flow of air to the cylinder was reinitiated immediately after the coverglass was withdrawn from the solution. The coverglasses were dipped only once. The excess CA was removed from the end of the coverglass with a cotton swab saturated with chloroform. Analysis of CA coated glass (not thermally annealed) and annealed commercial CA membranes by

atomic force microscopy (AFM) revealed similar but not identical surface morphologies (see Figure 4). Due to the lack of thermal annealing, the simulated CA 'membrane' is presumed to be structurally symmetrical, with high flux and poor solute rejection properties compared to commercial membranes.

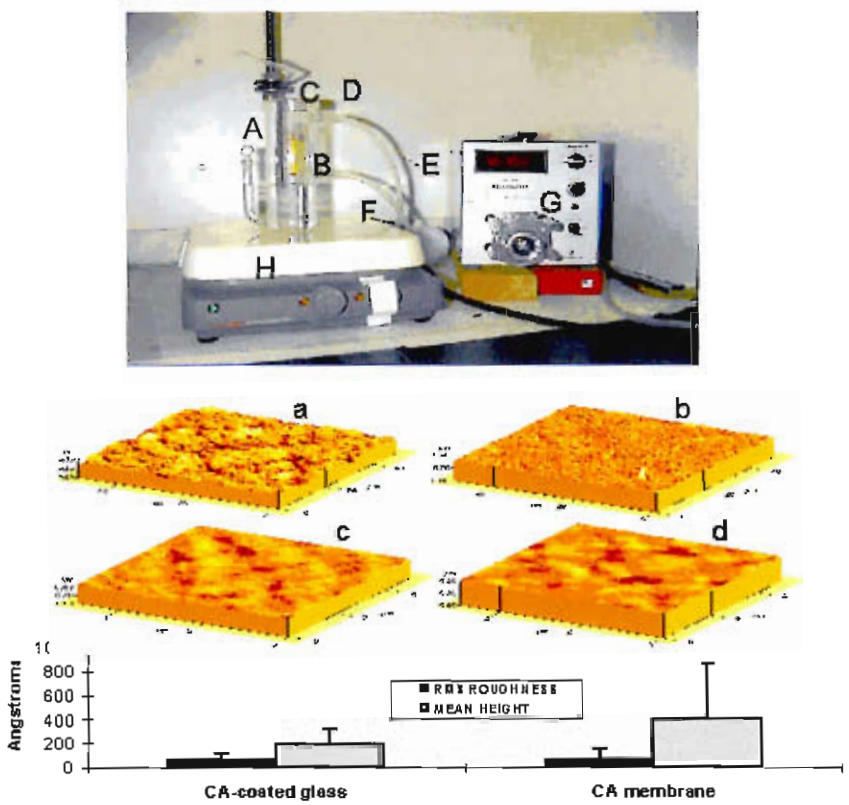

Figure 4. Upper panel: apparatus for casting CA thin films on coverglasses. (A) coating cylinder, (B) coverglass, (C) fine copper wire (connecting to coverglass), (D) nylon monofilament, (E) brass swivels, (F) dry air inlet/outlet lines (G) peristaltic pump, (H) stir plate. Middle panel: AFM images of commercial CA membrane at low (a) and high magnification (c); and CA thin film cast on glass at low (b) and high magnification (d). Lower panel: AFM height and roughness data for CA-coated glass and commercial CA membranes.

Real-time visualization and quantification of bacterial adhesion using microscope flow cells. A custom MFC design that has worked well with the fluorescence deconvolution microscope system (described above), consists of round upper (top) and lower (base) stainless-steel plates, each possessing optically transparent glass windows for viewing by transmitted light or epi-illumination (Figure 5). The window of the lower plate consists of a round 47 mm diameter coverglass of standard thickness (~170 μm) which seats into a precision machined circular recess (of the same depth) in the base plate. The dimensions of the MFC are such that it mates directly with the

stage of an Olympus inverted (IX70) or upright (AX70) microscope (see Figure 5b). When using an inverted microscope, the objective lens is moved into position directly beneath the base plate (coverglass) window. The coverglass may be used without any modification, but for membrane studies it was coated with a layer of CA, PA, or other polymer to simulate as closely as possible an actual membrane surface (see preceding section for a description of the coating process for CA films).

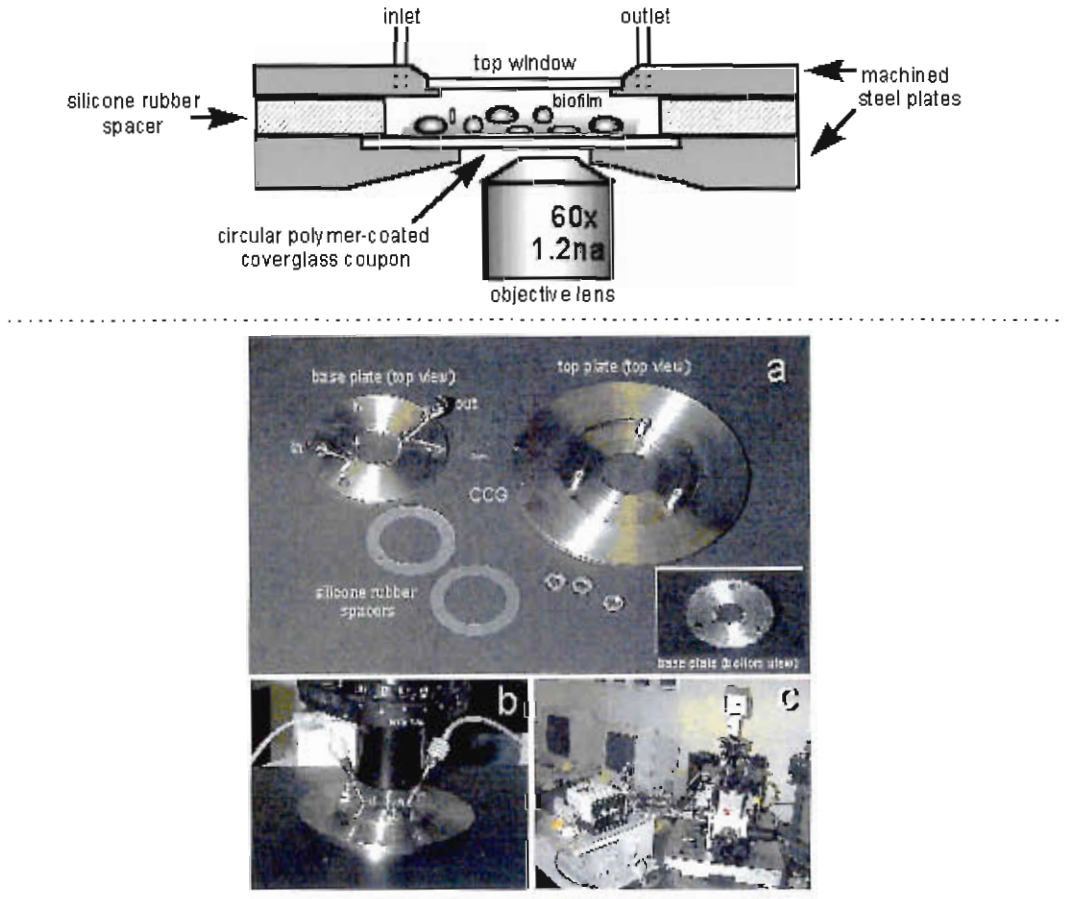

Figure 5. Upper panel: schematic of basic MFC construction and flow pattern. Lower panel: photographs of MFC components disassembled (a), MFC mated to inverted microscope stage (b), and MFC system integrated with microscope and peristaltic pump (c). CCG = circular polymer coated coverglass window.

The hydrodynamic properties of the MFC were calculated using standard fluid mechanic formulas (Figure 6) (17). The shape and dimensions of the flow channel (and hence the flow characteristics) of the MFC are solely defined by the silicon rubber spacer used to

seal and separate the upper and lower stainless steel plates. Typically, a 1.46 cm x 2.22 cm x 100 μm thick channel spacer was employed at flow rates of 0.05 to 1.0 mL/min. At these loading rates and spacer thicknesses, the calculated Reynolds number is <<1.0; thus, flow is considered to be laminar at the polymer film surface. Dye injection experiments conducted using the MFC confirmed the laminar nature of the flow over the range of spacer thickness and loading rates employed (data not shown).

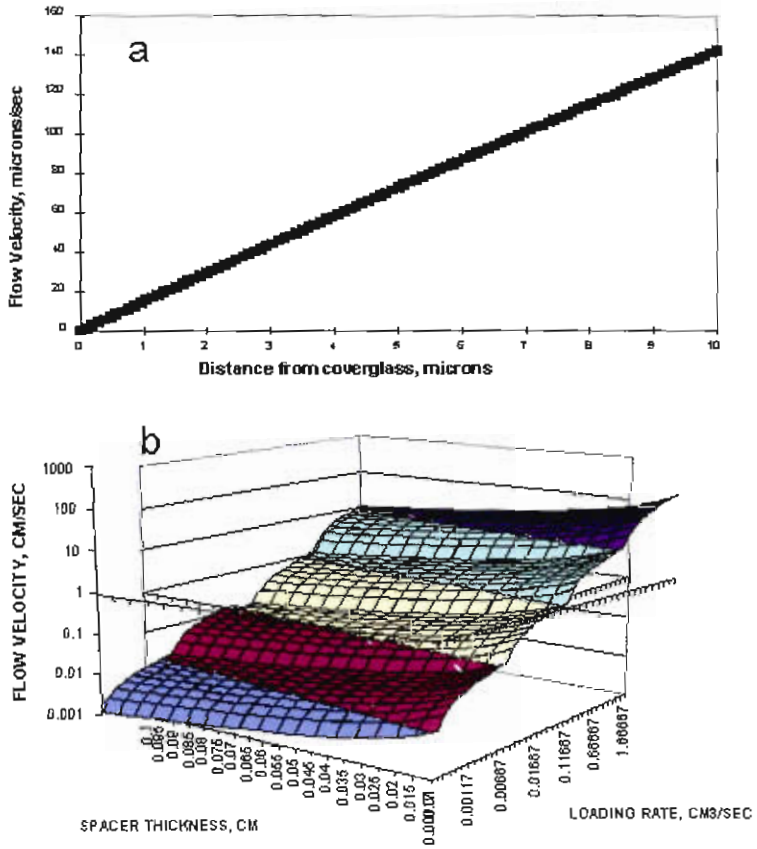

Figure 6. Calculated hydrodynamics of the MFC described in text. Note that flow velocity is linear over the range of 0-10 μm from the coupon surface for a rectangular flow channel with dimensions 1.46 cm x 2.22 cm x 100 μm (a). Early membrane biofilms typically fall well within this thickness range. MFC flow velocity is a function of spacer thickness and loading rate as indicated (b).

Operation of the MFC and general experimental protocols.

Detachment Experiments. For operation of the MFC, the polymer film on the coverglass surface was completely hydrated and pre-conditioned by introducing a suitable buffer solution (e.g., sterile-filtered MS buffer) (See Table 1) via syringe or

peristaltic pump. The buffer solution was typically pumped through the MFC for a period of no less than 15 minutes (at room temperature; ~23^{o}C), although the exact time depended on the specific swelling characteristics of the polymer film under investigation. Following complete hydration of the membrane substratum, an axenic bacterial suspension (about 10^8 cells/ml) was introduced via syringe pump or peristaltic pump into the MFC for a period of at least one hour or until bacterial attachment to the membrane surface occurred.

Table 1. Formulation of adhesion assay (AA) buffer* and AA growth medium*

Component	Amount
Na_2HPO_4	0.75 g/L
K_2HPO_4	0.75 g/L
NH_4Cl	1.0 g/L
$MgSO_4$-$7H_2O$	50 mg/L
$CaCl_2$-$2H_2O$	0.011 g/L
trace metals	600 µl/L
mannitol	1.0 g/L
pH adjusted to 7.2 prior to autoclaving	

*AA buffer contained no mannitol; **AA buffer containing mannitol is designated 'AA growth medium'

The test bacterium was either *Mycobacterium* strain BT2-4 or BT12-100, both of which were isolated from actual CA membrane biofilms from Water Factory 21, a 15 mgd wastewater reclamation facility located in Fountain Valley, CA. Both of these bacterial strains have been shown to possess similar surface hydrophobic and charge properties (data not presented). Bacteria were grown in AA buffer broth + 0.1 wt% mannitol for two days at 28°C prior to use in the above experimental protocol. Cells were washed twice in sterile nutrient free AA buffer immediately prior to use (See Table 2).

Table 2. Experimental parameters used for MFC biofilm growth and evaluation of test compounds in MFC

Parameter	Value or Description
test organism	*Mycobacterium* strains BT2-4 or BT12-100
growth medium	R2A (20) or AA buffer = 0.1 wt% mannitol (see Table 1).
growth incubation conditions	28°C, shaking at 200 rpm, 48 hours
cell harvesting	washed cells 2X in AA buffer by centrifugation at 10,000 rpm for 15 minutes
MFC experimental surface	unannealed CA polymer coated on optical coverglass from methylene chloride solution
typical MFC fluid loading rate	50µL/min
membrane surface pre-conditioning	continuous flow of sterile AA buffer for 10-30 minutes at RT (about 23°C) to hydrate CA surface
initial cell attachment	continuous flow of cell suspension in sterile AA buffer for 15-30 minutes or until stable attachment was observed
biofilm growth conditions	continuous flow of AA growth medium for 48 hours or until confluent coverage of membrane was achieved
test compounds	-anionic detergent dodecylbenzenesulfonic acid (DBSA) at 0.1, 0.05, 0.01 wt% and concentration gradient from 0-0.16 wt% continuous -sodium dodecyl sulfate (SDS) at 0.1% -anionic natural organic product zosteric acid at 0.1% -chloramine at 100 and 1000ppm -amphoteric surfactant/biocide Zwittergent 3-08 at 0.1 wt% -amphoteric surfactant/biocide Zwittergent 3-12 at 0.1 wt% -amphoteric surfactant/biocide Zwittergent 3-16 at 0.1 wt% -neutral polyoxyethylene detergent Triton X-100 concentration gradient from 0-0.15% continuous
Buffer system for test compounds	sterile AA buffer at pH 7.2
test compound contact time	typically 6 hours, but as long as 24 hours

Following initial bacterial attachment to the membrane surface, a sterile nutrient solution (AA buffer + 0.1 wt% mannitol) was introduced into the MFC (See Table 2 for protocol specifications). The MFC was operated in a continuous flow mode (50 microliters/minute) with mannitol supplementation for a period of approximately 48 hours or until confluent cell coverage was attained.

Native mixed species biofilms were constructed by feeding the MFC with secondary treated wastewater (Q1 water) for 48 hours.

Experimental cleaning agents or biocides were subsequently flushed (by sterile AA buffer) from the biofilm and test chemicals were introduced in a continuous flow mode to determine how the biofilm would respond. A region of interest was selected and images were digitally captured at predetermined intervals to document the test chemical's effects over time.

In order to more accurately establish the concentration at which different chemicals promoted cellular detachment from a CA membrane, an MFC experiment was performed in which the amount of detergent was varied continuously over a concentration gradient from 0 to 0.2 wt%. A gradient maker was utilized consisting of a scintillation vial (completely filled with AA buffer) with a septum cap pierced by two 22-gauge needles. One needle introduced the concentrated chemical into the gradient maker, and the other released the diluted solution out and into the MFC.

Attachment Experiments. Experiments were carried out where certain chemicals were used to pre-treat the CA-coated coverglass surface to determine whether *Mycobacterium* strain BT2-4 or BT12-100 cell attachment could be prevented or otherwise influenced by chemical pre-treatment prior to introduction of washed cells in AA buffer (nutrient free). The CA membrane was exposed to the chemical for a period of one hour followed by a brief rinse in AA buffer and introduction of *Mycobacteria* (about 10^8 cells/mL). Cell attachment was recorded by digitally photographing the visual appearance of the cells within a selected region of interest over time.

Biofilm Architecture. The structure of native biofilms formed either on actual RO membranes (cellulose acetate and polyamide) or on CA-coated coverglasses were examined. Native biofilms on actual RO membranes were developed by placing membrane samples from a reverse osmosis test unit that had been running for several (5–8) months on reverse osmosis feed water in the MFC for staining with the DNA-

Experimental cleaning agents or biocides were subsequently flushed (by sterile AA buffer) from the biofilm and test chemicals were introduced in a continuous flow mode to determine how the biofilm would respond. A region of interest was selected and images were digitally captured at predetermined intervals to document the test chemical's effects over time.

In order to more accurately establish the concentration at which different chemicals promoted cellular detachment from a CA membrane, an MFC experiment was performed in which the amount of detergent was varied continuously over a concentration gradient from 0 to 0.2 wt%. A gradient maker was utilized consisting of a scintillation vial (completely filled with AA buffer) with a septum cap pierced by two 22-gauge needles. One needle introduced the concentrated chemical into the gradient maker, and the other released the diluted solution out and into the MFC.

Attachment Experiments. Experiments were carried out where certain chemicals were used to pre-treat the CA-coated coverglass surface to determine whether *Mycobacterium* strain BT2-4 or BT12-100 cell attachment could be prevented or otherwise influenced by chemical pre-treatment prior to introduction of washed cells in AA buffer (nutrient free). The CA membrane was exposed to the chemical for a period of one hour followed by a brief rinse in AA buffer and introduction of *Mycobacteria* (about 10^8 cells/mL). Cell attachment was recorded by digitally photographing the visual appearance of the cells within a selected region of interest over time.

Biofilm Architecture. The structure of native biofilms formed either on actual RO membranes (cellulose acetate and polyamide) or on CA-coated coverglasses were examined. Native biofilms on actual RO membranes were developed by placing membrane samples from a reverse osmosis test unit that had been running for several (5–8) months on reverse osmosis feed water in the MFC for staining with the DNA-specific dye propidium iodide (PI, Sigma, St. Louis, MO), a fluorochrome that binds to nuclear material (DNA) and fluoresces red when excited by green light. CA-coated

coverglasses were placed in the MFC and exposed to secondary-treated sewage effluent at WF-21 for 48 hours, and then brought to the laboratory for staining with PI and microscopic observation. Monospecies biofilms of *Mycobacterium* were also formed on CA-coated coverglasses (as previously described).

Dual staining experiments were performed in order to qualitatively and quantitatively describe the distribution of cells and exopolymer in the biofilms. The bacteria were stained with PI and the exopolymeric substances (EPS) was differentially stained with Fluorescent Brightener 28 (calcofluor white, Sigma, St. Louis, MO), an organic compound that binds to polysaccharides and exhibits a blue-white fluorescence. In order to quantify the distribution of cells and EPS in a biofilm volume, a series of equidistant (1-voxel) slice planes projected through the biofilm specimen along the 'z' axis was created. Fluorochrome distribution was determined at each slice plane using image analysis (Image-Pro Plus).

Latex FluoSpheres, amidine, (0.5 µm, Molecular Probes Inc., Eugene, OR) were used to visualize void spaces and channels within the biofilms. The beads were suspended in buffer and introduced into the MFC via a syringe or peristaltic pump.

All the biofilms were subsequently imaged using green light excitation (about 530 nm) to visualize the propidium iodide under a 100x high-aperture oil immersion objective lens. Flash duration was approximately 100 µsec and about 16 flashes per optical section were averaged. UV light was used to visualize the beads. Typically, about 50-100 optical sections were captured for each biofilm specimen. These stacks were reconstructed using a voxel reconstruction program and a 3D model of the biofilm generated.

Membrane Surface Charge. The attachment behavior of polysterene latex microspheres (PLMs) carrying positive or negative surface charges to membranes was studied to get information about membrane surface charge distribution. Small pieces of polyamide membrane were immersed in two different types of PLMs solutions to

observe the binding of the charged beads to the membrane. The positively-charged PLMs (FluoSpheres, amidine, 0.5 µm, Molecular Probes, Inc., Eugene, OR) and negatively-charged PLMs (FluoSpheres, carboxylate-modified, 1.0 µm, Molecular Probes, Inc., Eugene, OR) were diluted in HEPES buffer, pH=7, brought to a volume of 10 mL in scintillation vials. The membrane coupons were immersed in these solutions for about one hour. The membrane coupons were rinsed in HEPES buffer by gentle agitation, and were then mounted on microscope slides for observation under UV epi-illumination.

The effect of pH and ionic strength on binding of amidine beads to polyamide membranes were studied by immersing membrane coupons into solutions containing amidine beads (100 µL) in 10 mL of different pH solutions (2, 4, 7, and 10), or different NaCl concentrations (0, 0.01, 0.1, 0.5, and 1.0 M) prepared in HEPES buffer. Controls contained the beads in 10 mL of HEPES buffer alone.

RESULTS

Membrane Surface Structure.

Membrane Surface Charge Distribution. The surface charge characteristics of polymeric membranes are dependent on the chemical properties of the membrane and the chemistry of the solution (6). The attachment behavior of polystyrene microspheres (PLMs) carrying positive (amidine) or negative (carboxylated) surface charge to membranes was studied in order to determine membrane surface charge distribution. Amidated (positive) PLMs were found to undergo extensive but extremely uneven binding to actual CA membrane surfaces, whereas carboxylated PLMs failed to adsorb or adsorbed very poorly by comparison (Fig. 7). Furthermore, PLM adsorption was observed to increase where surface topographic defects such as scratches or abrasions occurred.

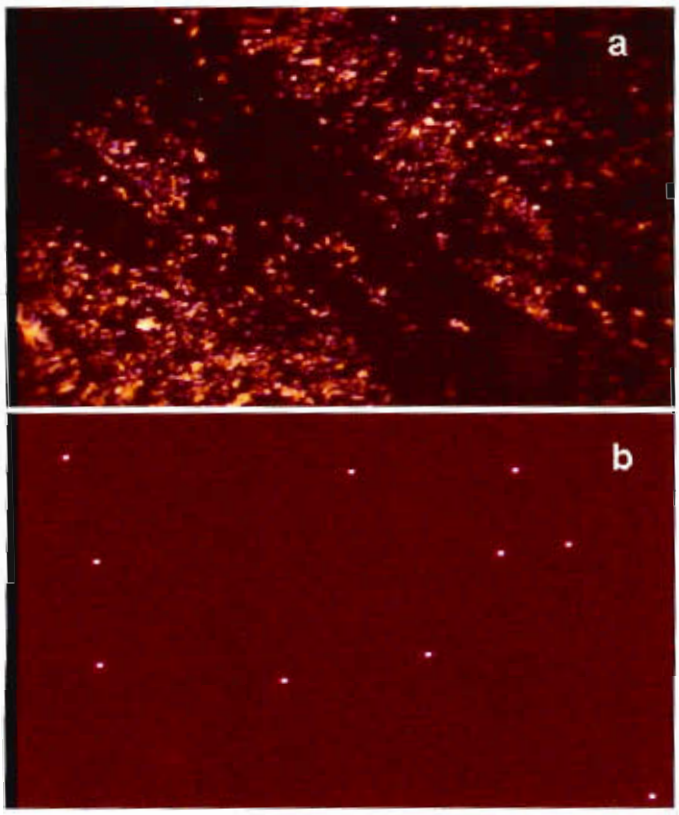

Figure 7. Adsorption behavior of amidated (a) and carboxylated (b) PLMs to an actual CA membrane. Note extensive and uneven binding of positive charged amidated PLMs compared to negative charged carboxylated PLMs.

The ionic strength of the aqueous environment did not influence the binding behavior of the PLMs to either the CA or PA membrane surfaces; no effect was observed with NaCl concentrations varying from 0 mM to 1000 mM. Likewise, varying the pH from 2 to 12 had no effect on PLM binding to either PA or CA membranes (Data not shown).

Biofilm Architecture. A selected series of 3D reconstructions of natural 5-8 month old multi-species membrane biofilms grown on polyamide membranes (FT-30) from actual reverse osmosis plant feedwater is presented in Figures 8-13. In each case, the biofilm is presented in three different orientations (top view of stacked optical sections, oblique view, and cross-sectional views) to illustrate the overall arrangement of individual cells.

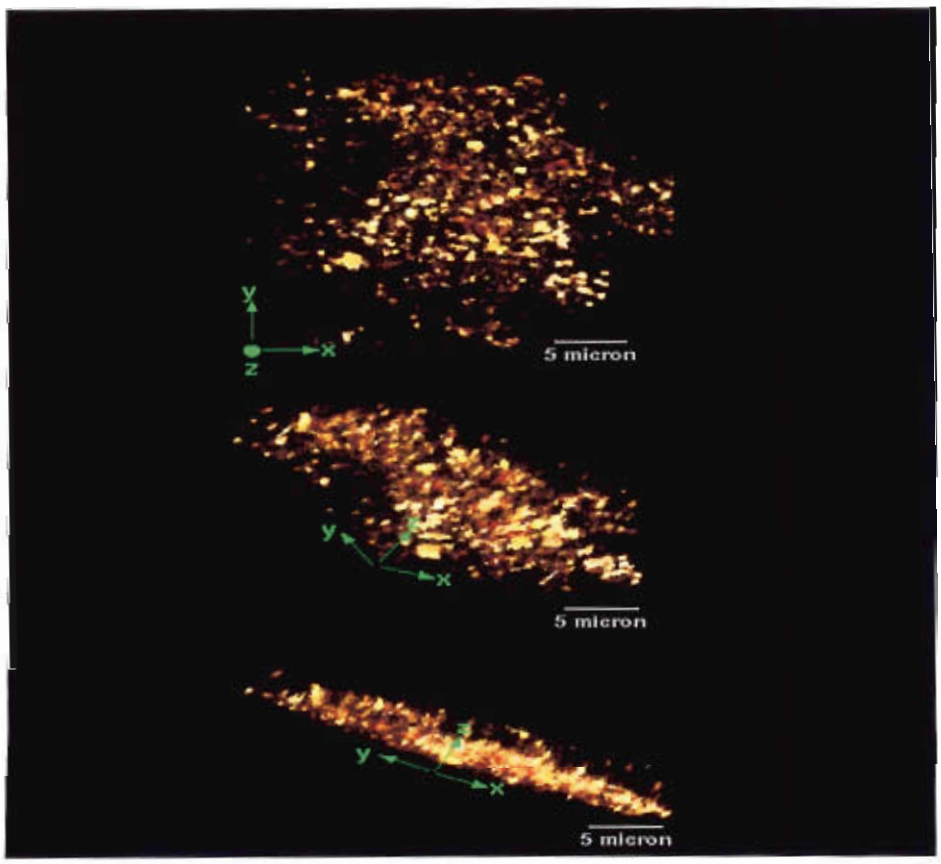

Figure 8. Natural biofilm grown on PA membrane stained with propidium iodide. Feed = conventional pre-treated RO feed; run time = 8 months.

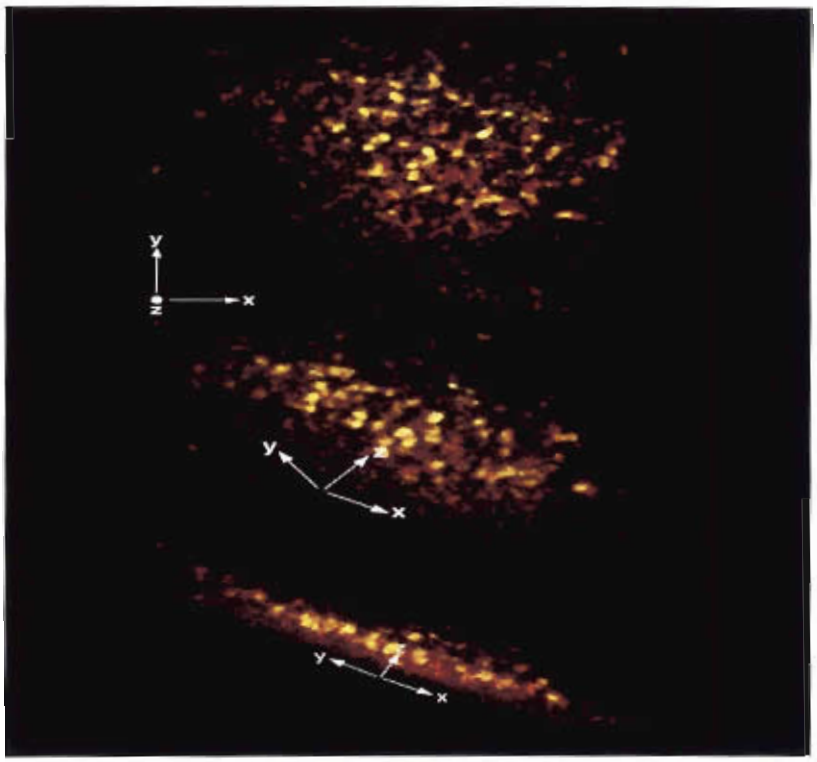

Figure 9. Natural biofilm grown on PA membrane stained with propidium iodide. Feed = conventional pre-treated RO feed; run time = 8 months.

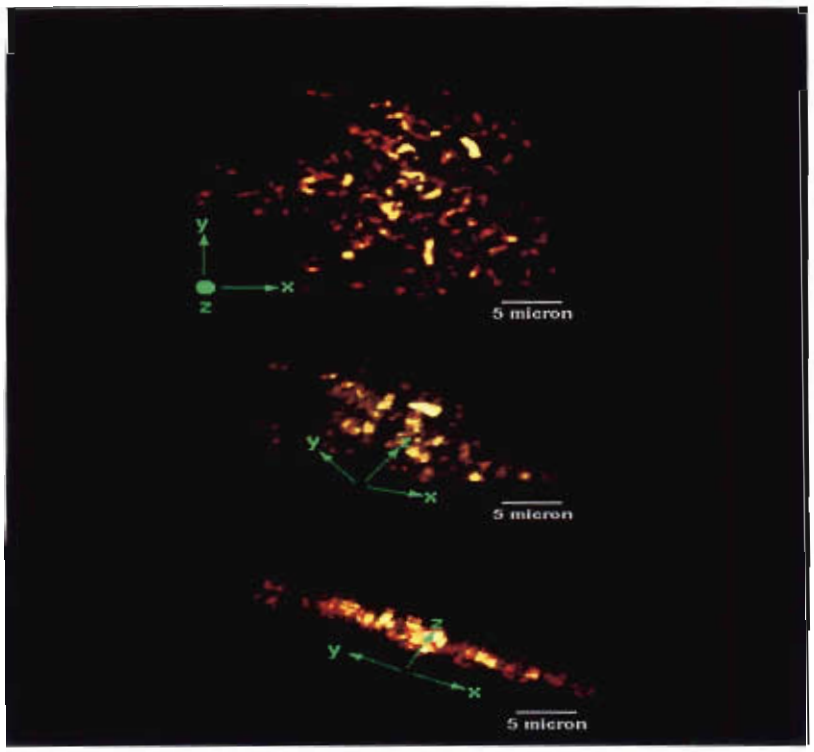

Figure 10. Natural biofilm grown on PA membrane stained with propidium iodide. Feed = conventional pre-treated RO feed; run time = 8 months.

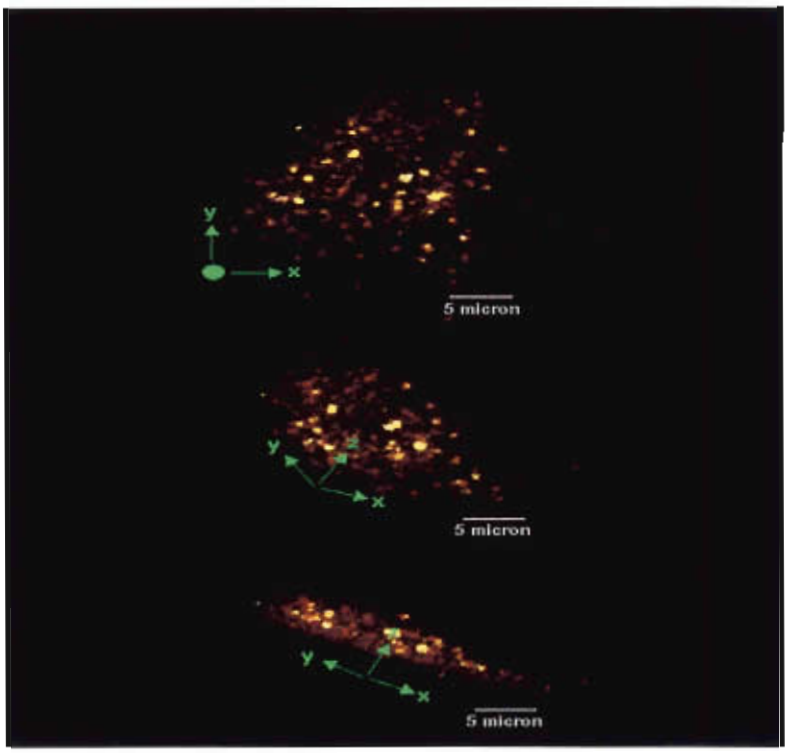

Figure 11. Natural biofilm grown on PA membrane stained with propidium iodide. Feed = conventional pre-treated RO feed; run time = 8 months.

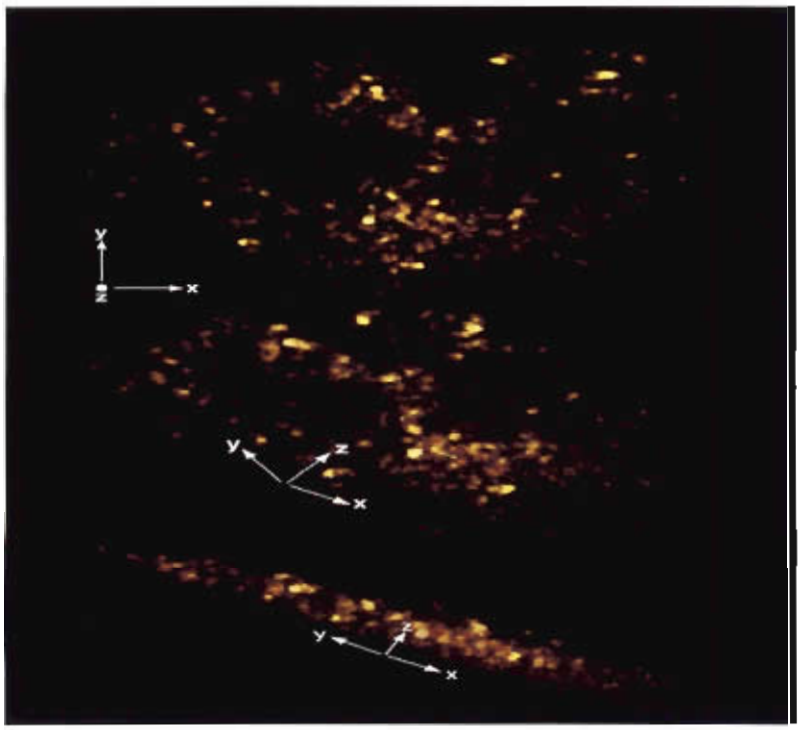

Figure 12. Natural biofilm grown on PA membrane stained with propidium iodide. Feed = conventional pre-treated RO feed; run time = 8 months.

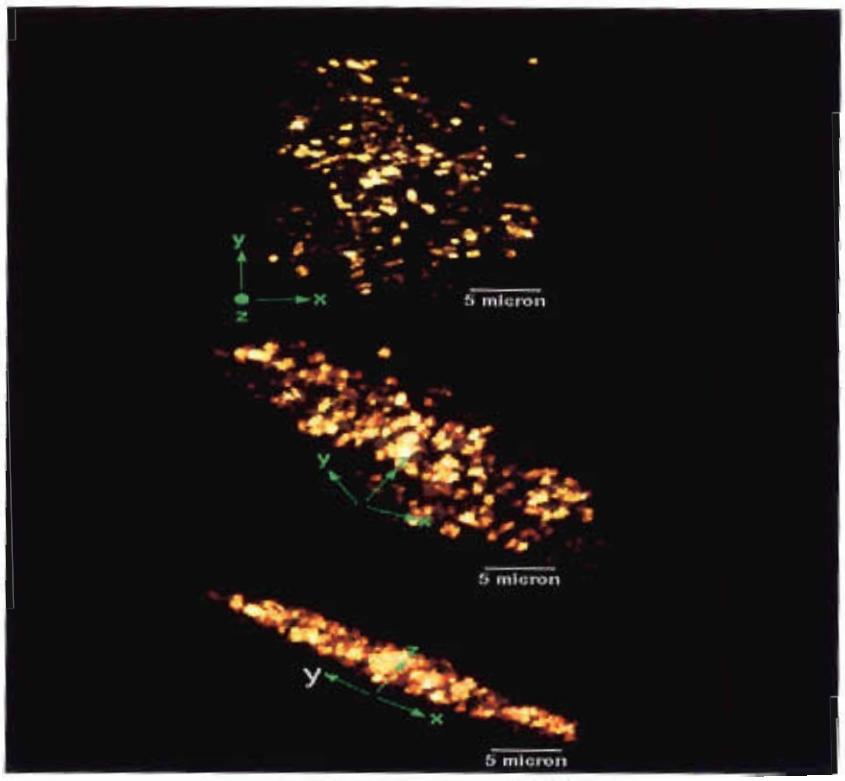

Figure 13. Natural biofilm grown on PA membrane stained with propidium iodide. Feed = conventional pre-treated RO feed; run time = 8 months.

Several generalizations may be made regarding the structure of these membrane biofilms. The individual cells were not uniformly distributed; instead they were arranged in an uneven or patchy manner resulting in a high degree of spatial heterogeneity within the biofilm. Areas of dense population were often separated by apparently sparsely populated regions. Some of the more sparsely colonized areas extended for considerable distances through the interior of the biofilm (visible in some 3D reconstructions), thereby resembling "tunnels" or "channels" (Fig. 13). The overall thickness of the biofilms was typically about 5 microns, even though we have seen biofilms up to 20 microns thick. Finally, biofilms formed on CA membranes were essentially morphologically indistinguishable from those that were formed on polyamide membranes (Figs. 14-21). The cell distribution on CA and PA membrane biofilms was also very similar, showing the cells to be arranged generally between approximately 5 and 12-20 microns above the membrane surface. Some examples are shown in Fig. 22.

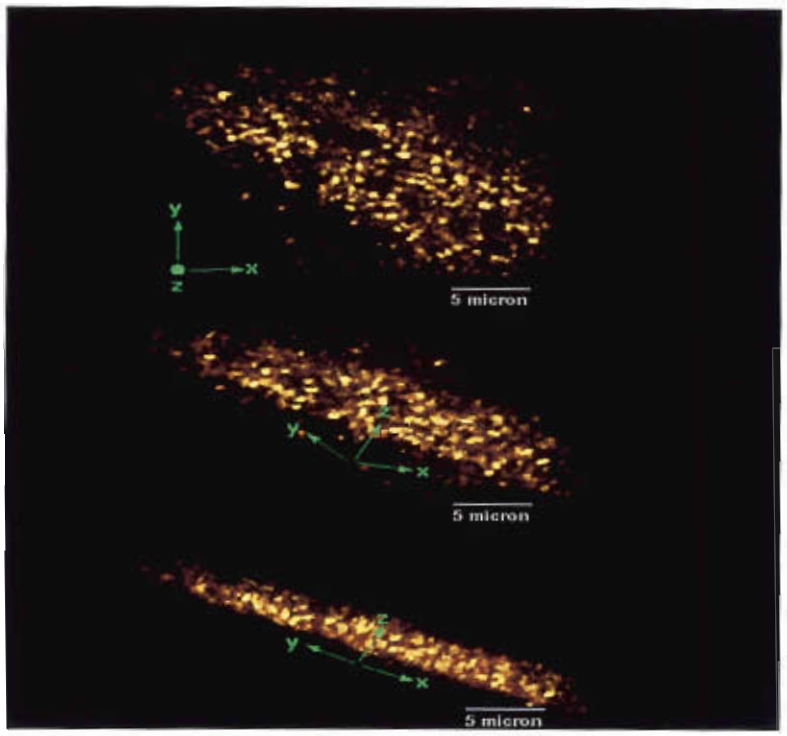

Figure 14. Natural biofilm grown on CA membrane stained with propidium iodide. Feed = conventional pre-treated RO feed; run time = 5 months.

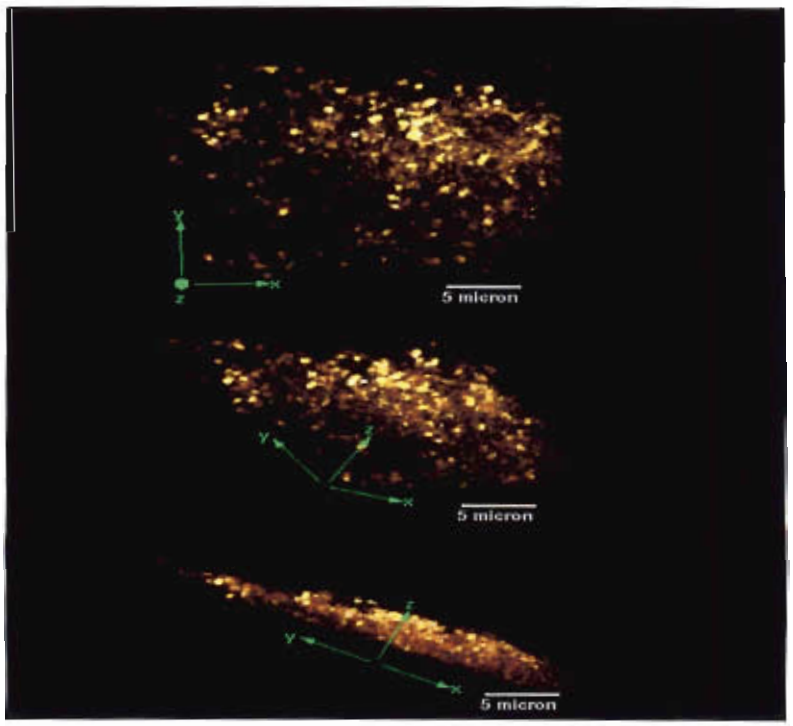

Figure 15. Natural biofilm grown on CA membrane stained with propidium iodide. Feed = conventional pre-treated RO feed; run time = 5 months.

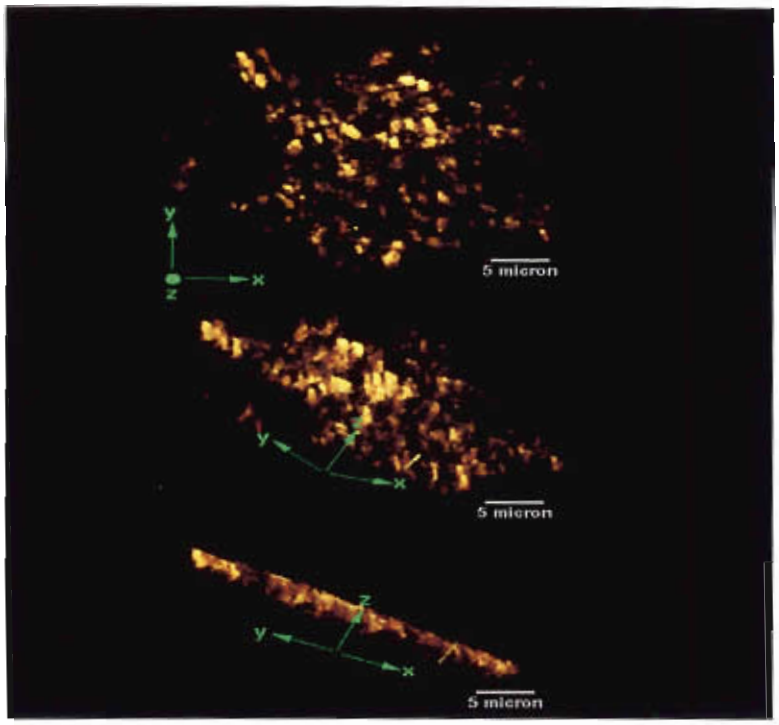

Figure 16. Natural biofilm grown on CA membrane stained with propidium iodide. Feed = conventional pre-treated RO feed; run time = 5 months.

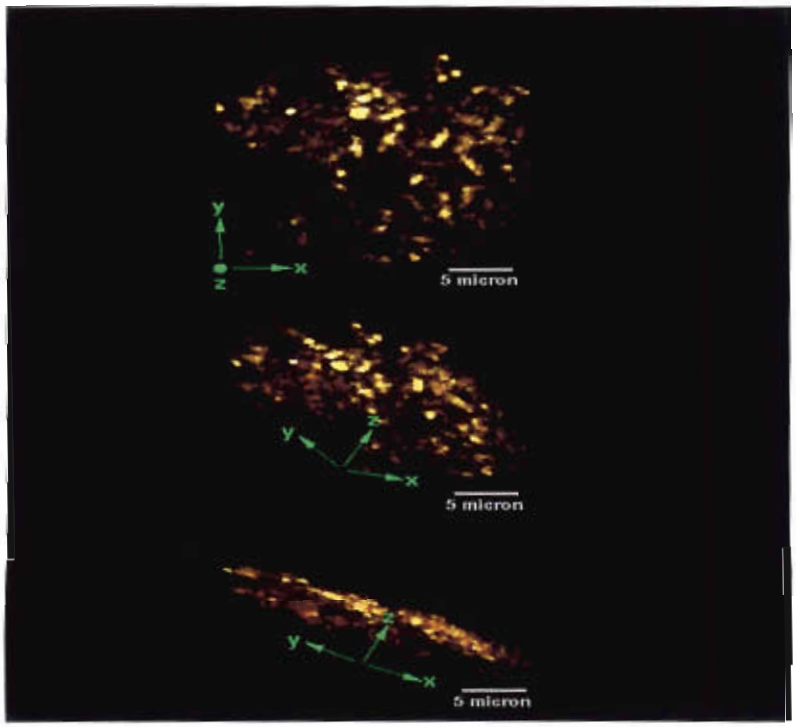

Figure 17. Natural biofilm grown on CA membrane stained with propidium iodide. Feed = conventional pre-treated RO feed; run time = 5 months.

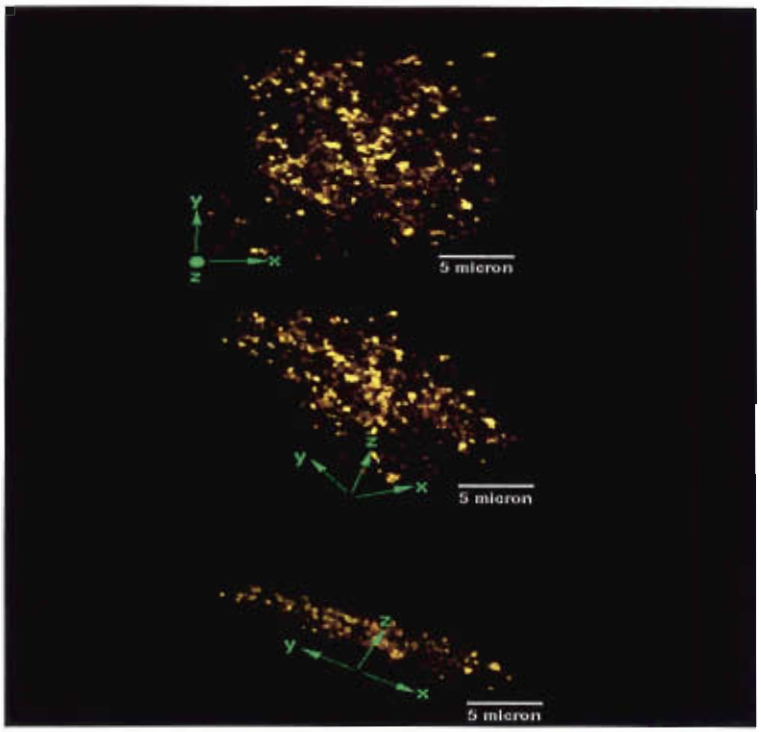

Figure 18. Natural biofilm grown on CA membrane stained with propidium iodide. Feed = conventional pre-treated RO feed; run time = 5 months.

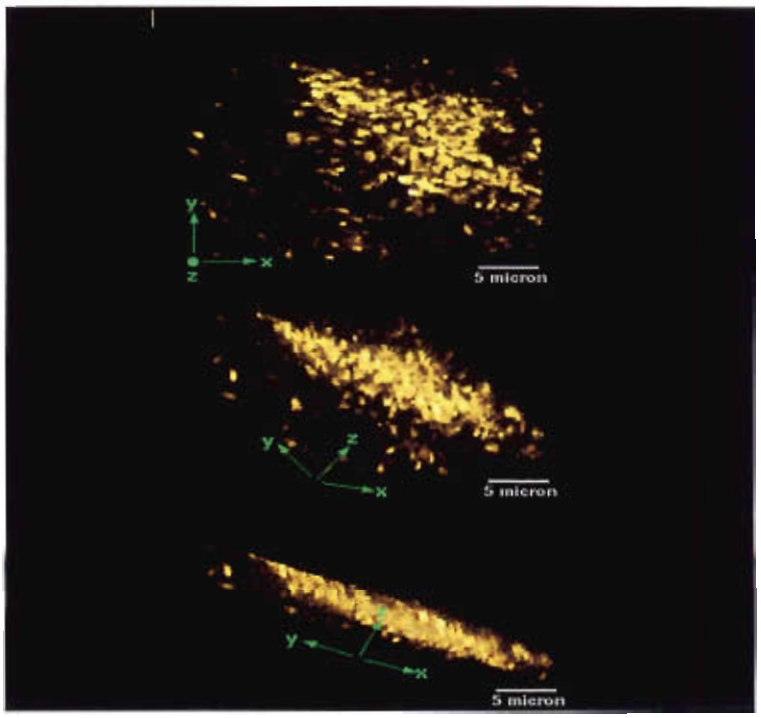

Figure 19. Natural biofilm grown on CA membrane stained with propidium iodide. Feed = conventional pre-treated RO feed; run time = 5 months.

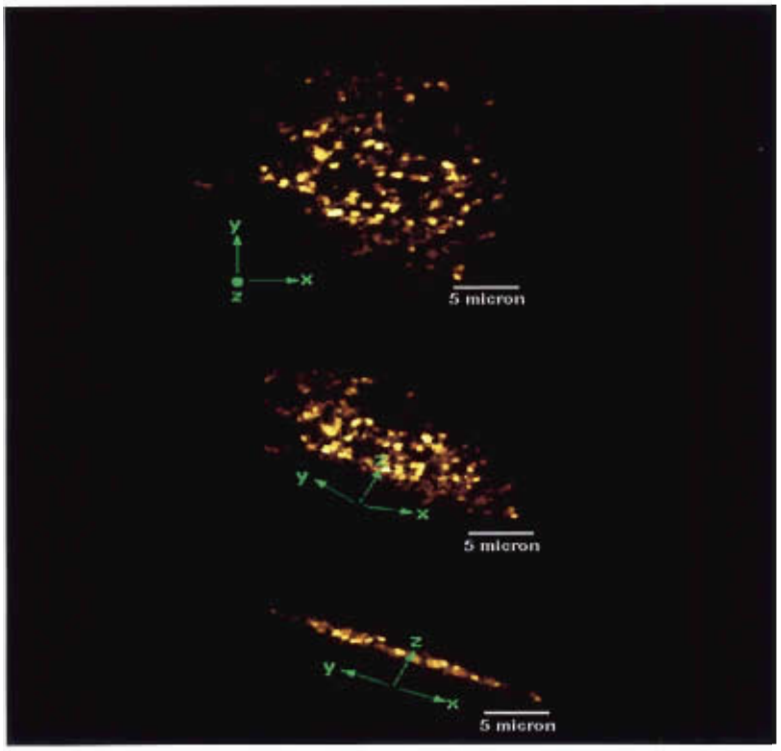

Figure 20. Natural biofilm grown on CA membrane stained with propidium iodide. Feed = conventional pre-treated RO feed; run time = 5 months.

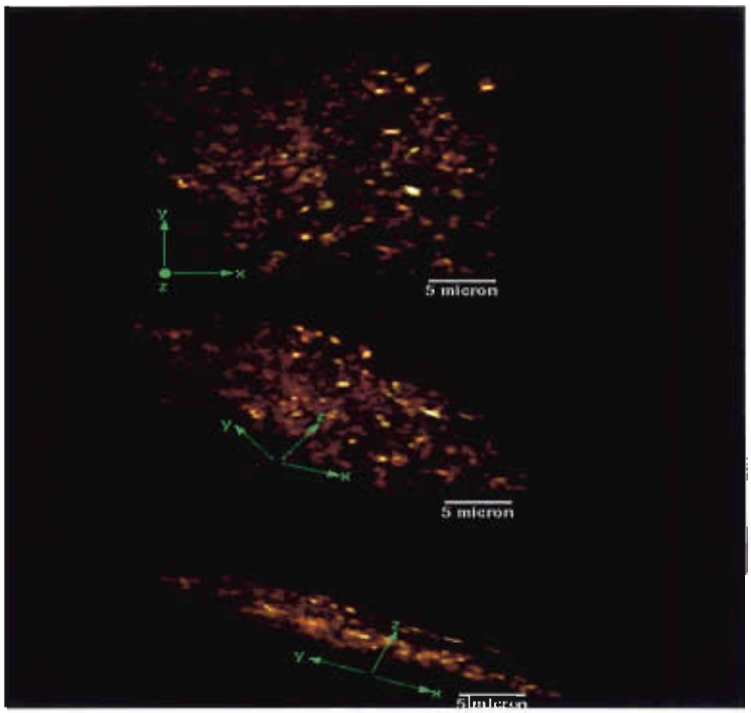

Figure 21. Natural biofilm grown on CA membrane stained with propidium iodide. Feed = conventional pre-treated RO feed; run time = 5 months.

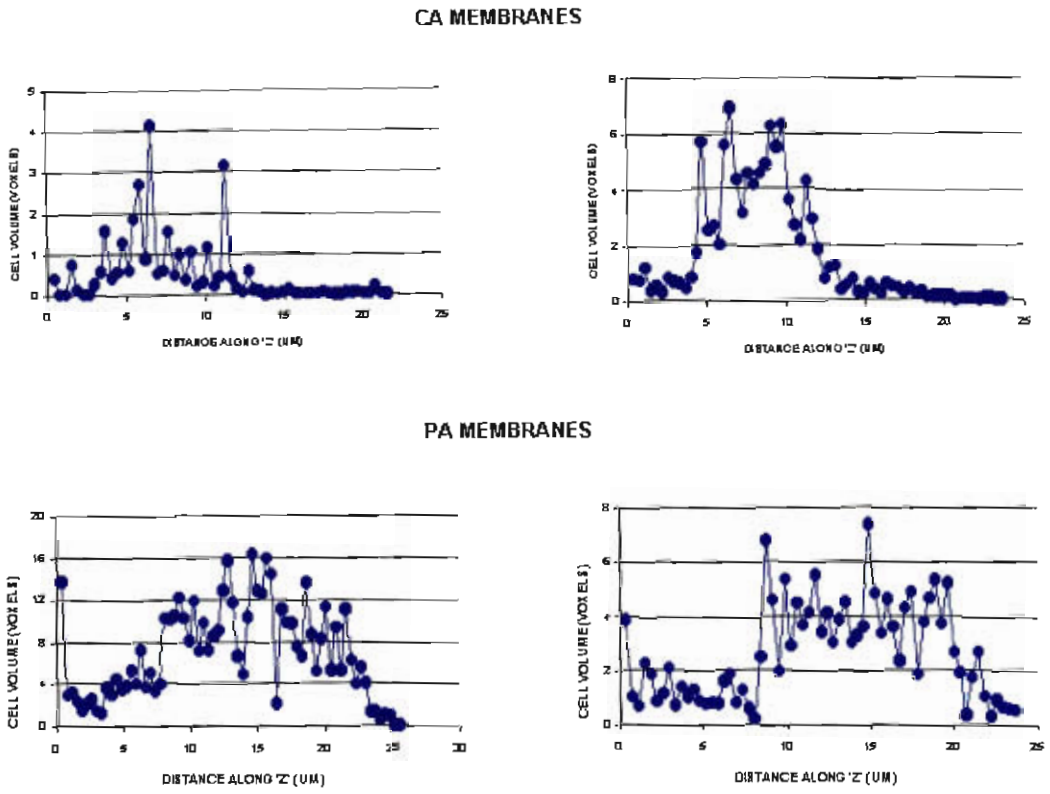

Figure 22. Distribution of bacterial cells along the 'z' axis of the total volume of the biofilms on CA and PA membranes.

Areas of the biofilm where cells were sparse (e.g., the "channels") sometimes contained a diffuse background of propidium iodide stain, suggesting the presence of extracellular polymeric substances (EPS).

Biofilms formed from secondary treated sewage effluent on CA-coated coverglasses *using the* MFC were also studied. They were very similar morphologically to those formed on actual RO membranes in terms of composition and thickness, but the arrangement seems to be more uniform across the coverglass, as opposed to the more irregular distribution that corresponded to the defects on the reverse osmosis membranes. (Figs. 23-27).

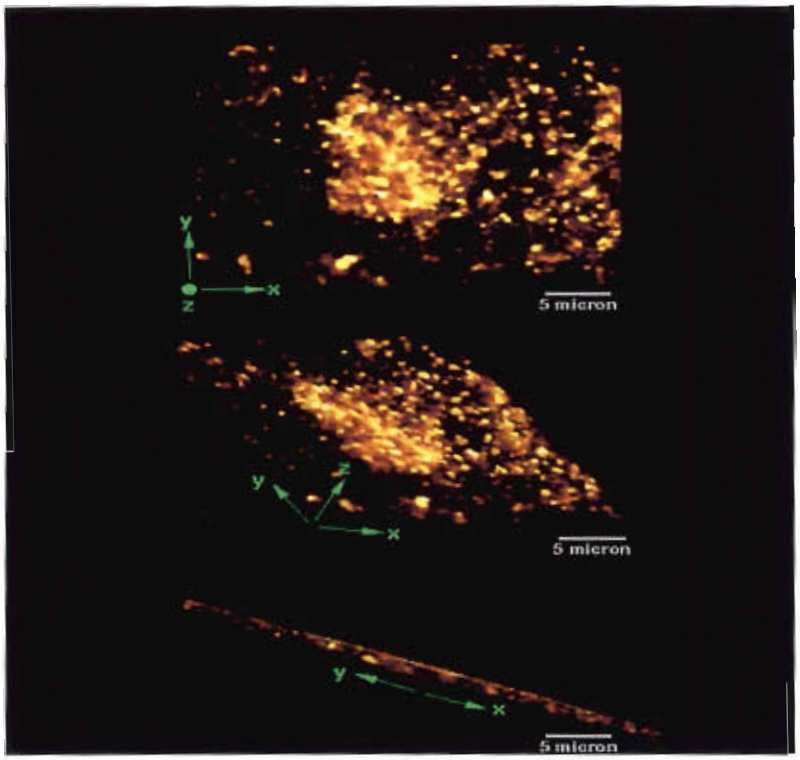

Figure 23. Natural biofilm grown on CA-coated coverglass stained with propidium iodide. Feed = secondary-treated wastewater; run time = 48 hours.

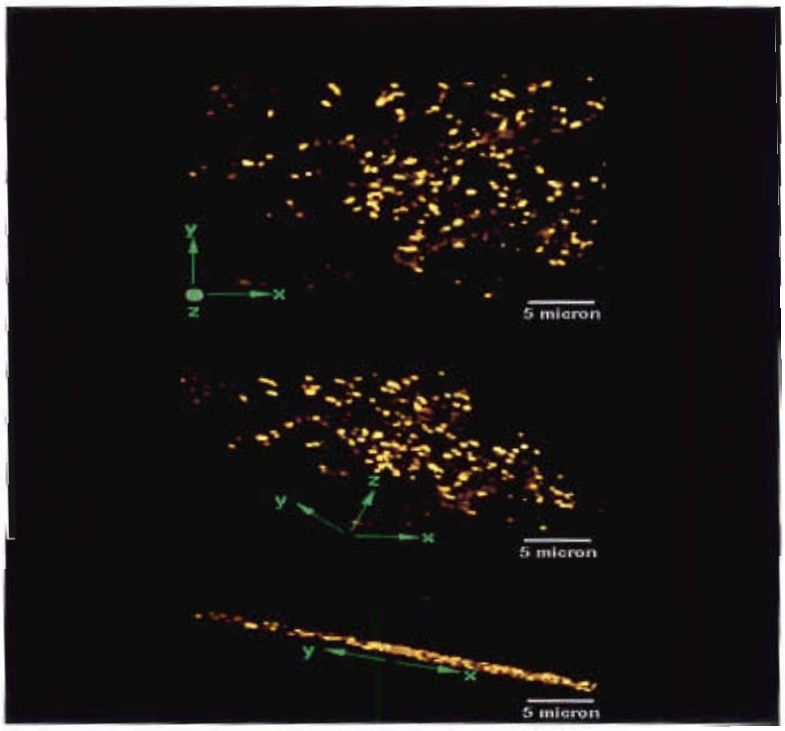

Figure 24. Natural biofilm grown on CA-coated coverglass stained with propidium iodide. Feed = secondary-treated wastewater; run time = 48 hours.

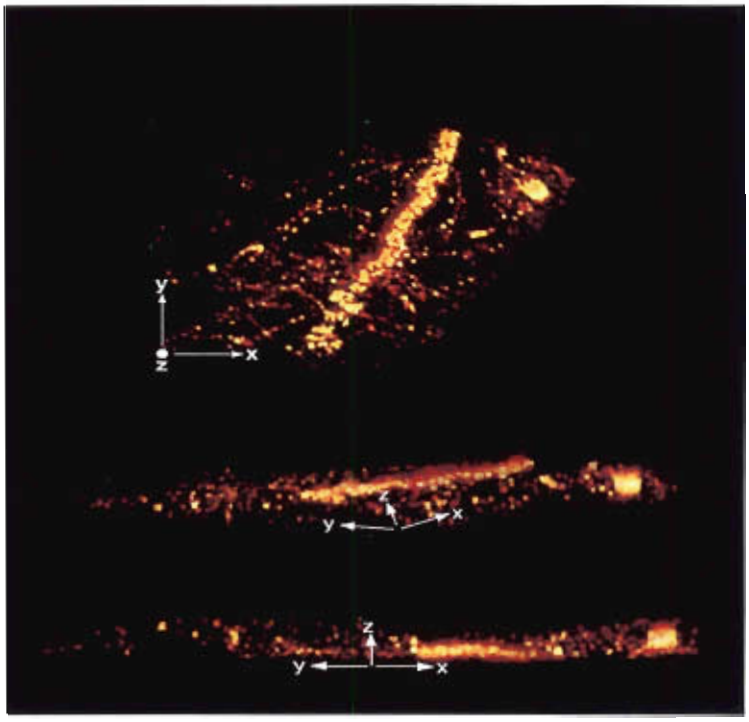

Figure 25. Natural biofilm grown on CA-coated coverglass stained with propidium iodide. Feed = secondary-treated wastewater; run time = 48 hours.

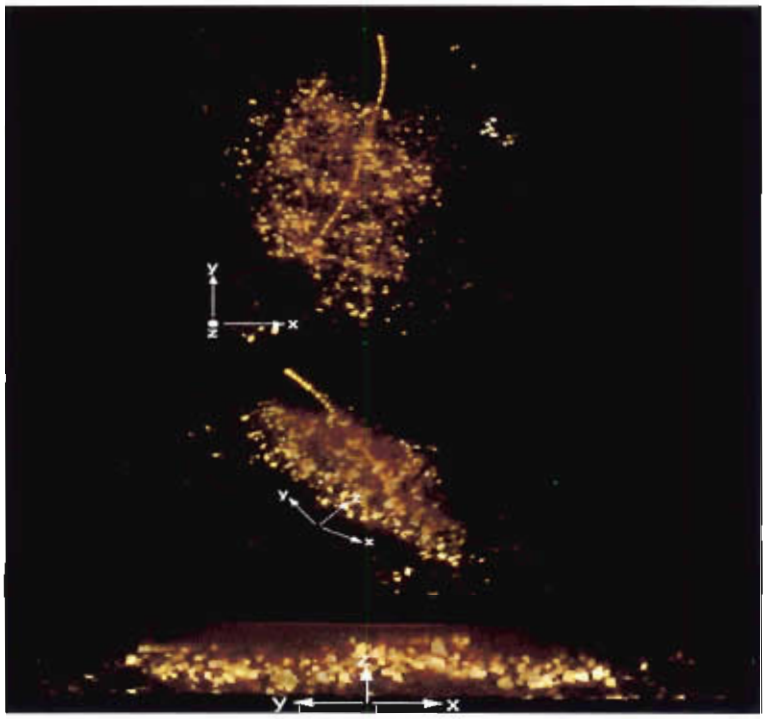

Figure 26. Natural biofilm grown on CA-coated coverglass stained with propidium iodide. Feed = secondary-treated wastewater; run time = 48 hours.

Figure 27. Natural biofilm grown on CA-coated coverglass stained with propidium iodide. Feed = secondary-treated wastewater; run time = 48 hours.

Cells in the natural biofilms formed on CA-coated coverglasses, and dual stained (PI and calcofluor white), appeared more concentrated in the middle of the volume than towards the coverglass surface or the top of the biofilm, while the exopolymer seemed evenly distributed throughout the biofilm along the 'z' axis (Figs. 28 and 30) . Data resulting from image analysis (Figs. 29 and 31) confirmed the usual observations regarding distribution of exopolymer and cells from the surface of the coverglass to the top of the biofilm.

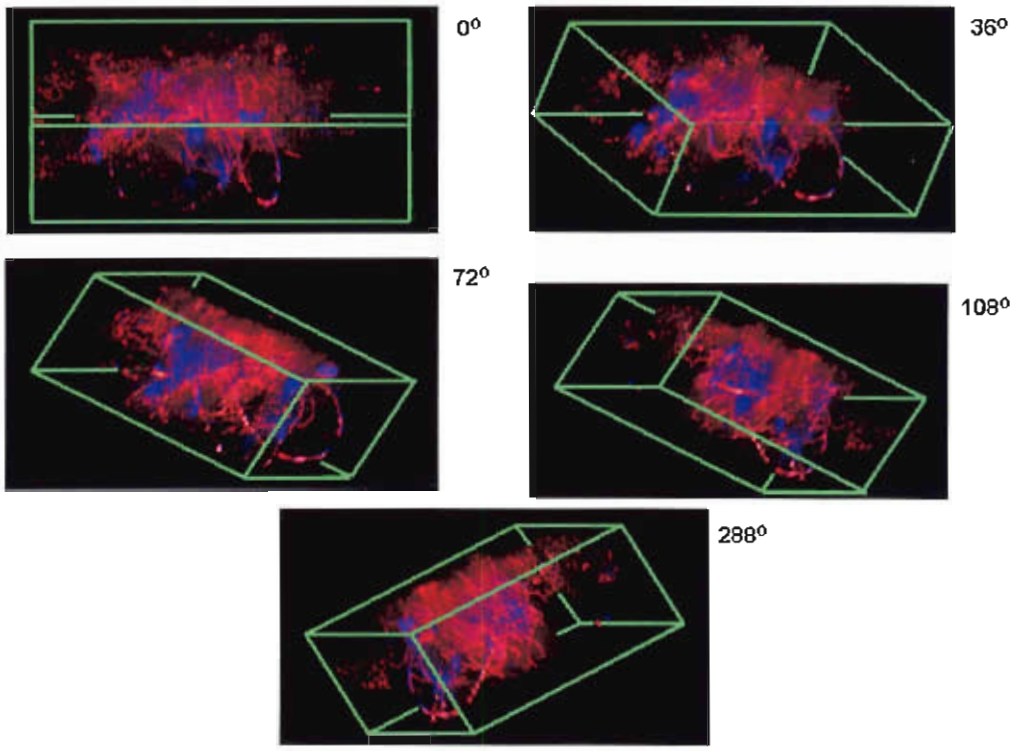

Figure 28. Five perspective views of a 4-day old native multi-species membrane biofilm reconstructed in 3D from 250 2D image sections. Red objects = individual bacteria stained with PI. Blue material = extracellular polymeric substances (EPS) differentially stained with calcofluor white. The biofilm thickness was 90 µm.

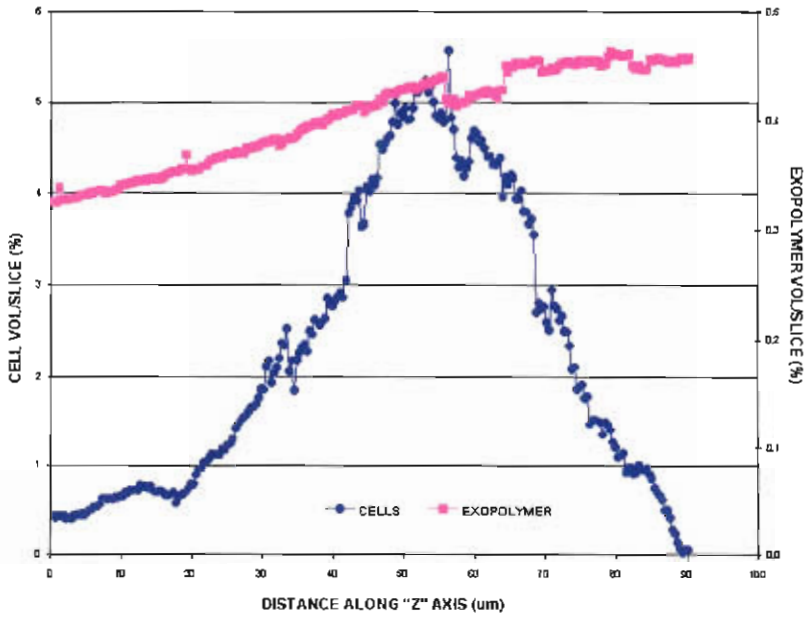

Figure 29. Distribution of bacterial cells and extracellular polymeric substances (EPS) along the 'z' axis of the total volume of the biofilm depicted in Fig. 28.

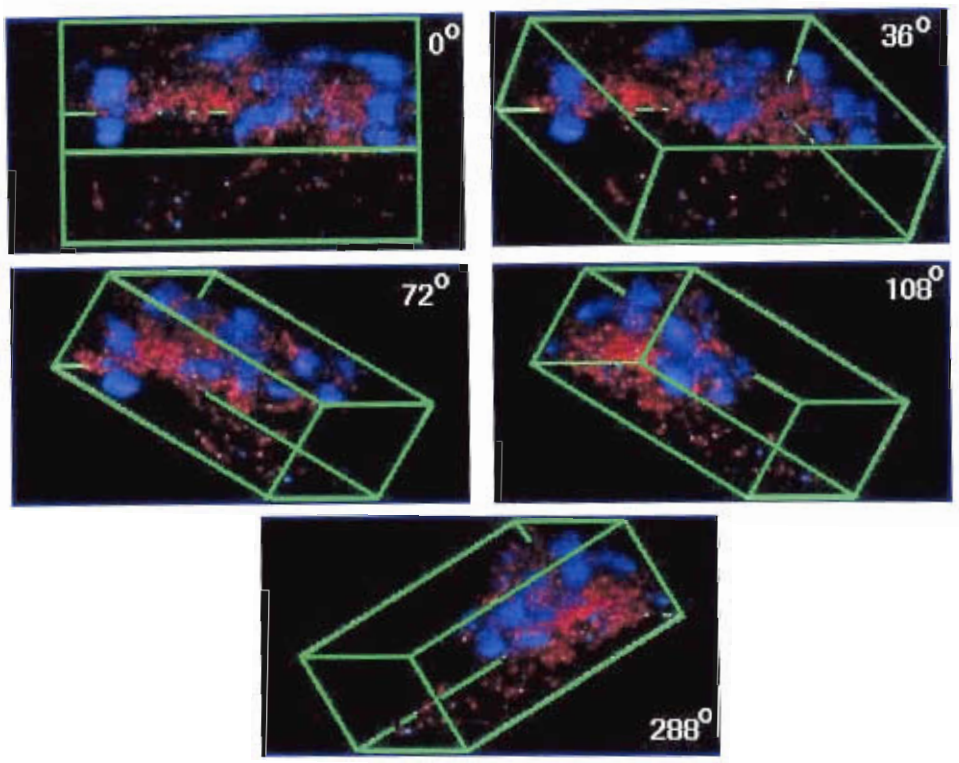

Figure 30. Five perspective views of a 3-day old native multi-species membrane biofilm reconstructed in 3D from 157 2D image sections. Red objects = individual bacteria stained with PI. Blue material = extracellular polymeric substances (EPS) differentially stained with calcofluor white. The biofilm thickness was 47 µm.

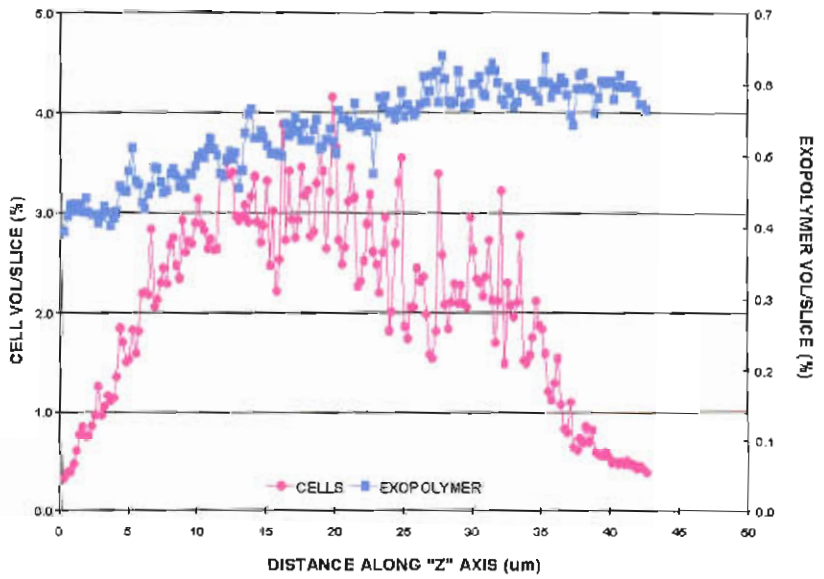

Figure 31. Distribution of bacterial cells and extracellular polymeric substances (EPS) along the 'z' axis of the total volume of the biofilm depicted in Fig. 30.

In another example, the cells were observed to be more concentrated towards the top of the biofilm and the exopolymer more concentrated on the surface of the membrane-coated coverglass (Figs. 32 and 33). In all cases, natural biofilms showed a tendency for greater biomass away from the surface.

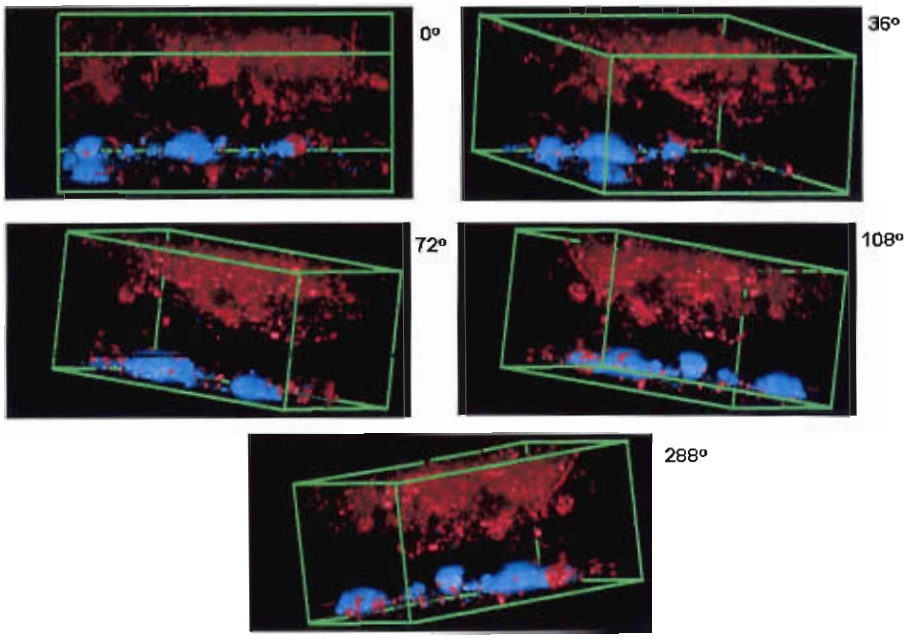

Figure 32. Five perspective views of a 3-day old native multi-species membrane biofilm reconstructed in 3D from 170 2D image sections. Red objects = individual bacteria stained with PI. Blue material = extracellular polymeric substances (EPS) differentially stained with calcofluor white. The biofilm thickness was 51 µm.

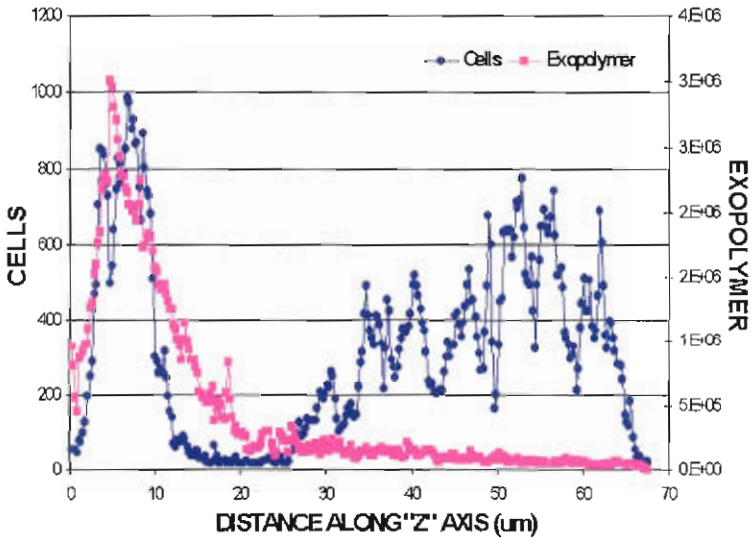

Figure 33. Distribution of bacterial cells and extracellular polymeric substances (EPS) along the 'z' axis of the total volume of the biofilm depicted in Fig. 32.

Biofilms of Mycobacterium strain BT12-100 also showed cells more concentrated away from the coverglass surface and the top of the biofilm (Figs. 34-36). As with the natural biofilm (Fig. 28), the cells were more concentrated in the middle of the biofilm volume, in between clouds of exopolymer that seemed to be evenly distributed across the biofilm.

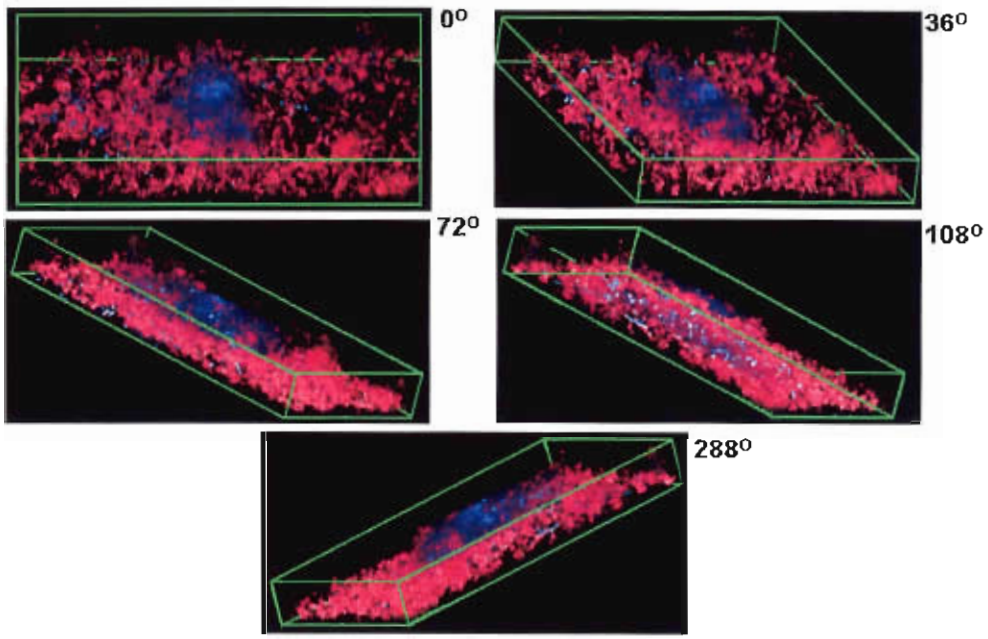

Figure 34. Five perspective views of a 48-hour old monoculture biofilm of *Mycobacterium* strain BT12-100 reconstructed in 3D from 50 2D image sections. Red objects = individual bacteria stained with PI. Blue material = extracellular polymeric substances (EPS) differentially stained with calcofluor white. The biofilm thickness was 15 µm.

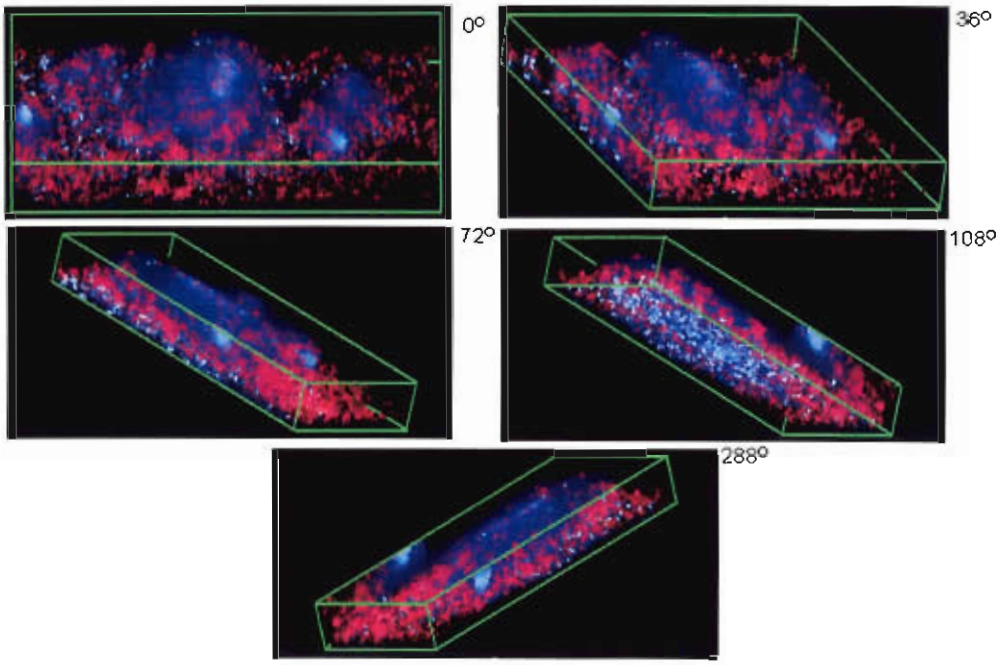

Figure 35. Five perspective views of a 48-hour old monoculture biofilm of *Mycobacterium* strain BT12-100 reconstructed in 3D from 57 2D image sections. Red objects = individual bacteria stained with PI. Blue material = extracellular polymeric substances (EPS) differentially stained with calcofluor white. The biofilm thickness was 14 µm.

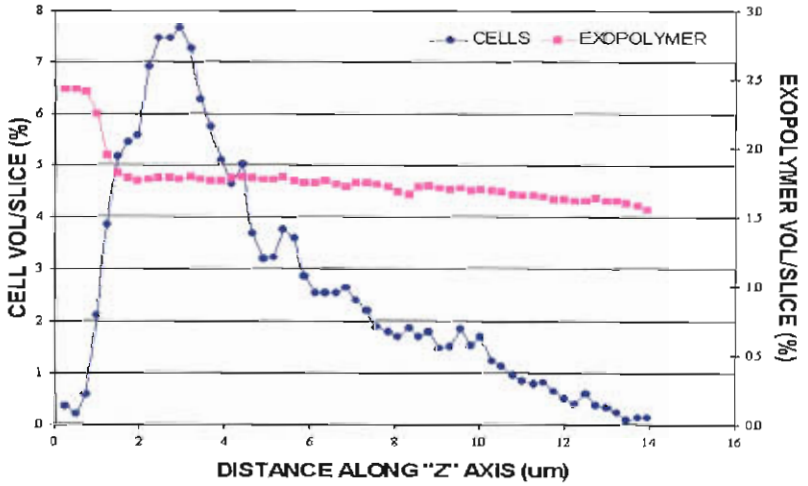

Figure 36. Distribution of bacterial cells and extracellular polymeric substances (EPS) along the 'z' axis of the total volume of the biofilm depicted in Fig. 35.

Fluorescent bead penetration experiments showed the beads attached mostly to the CA-coated membrane surface in regions lacking dense population of cells (Figs. 37 and

39). Data resulting from image analysis (Figs. 38 and 40) confirmed these observations regarding the distribution of the fluorescent beads from the surface of the coverglass to the top of the biofilm.

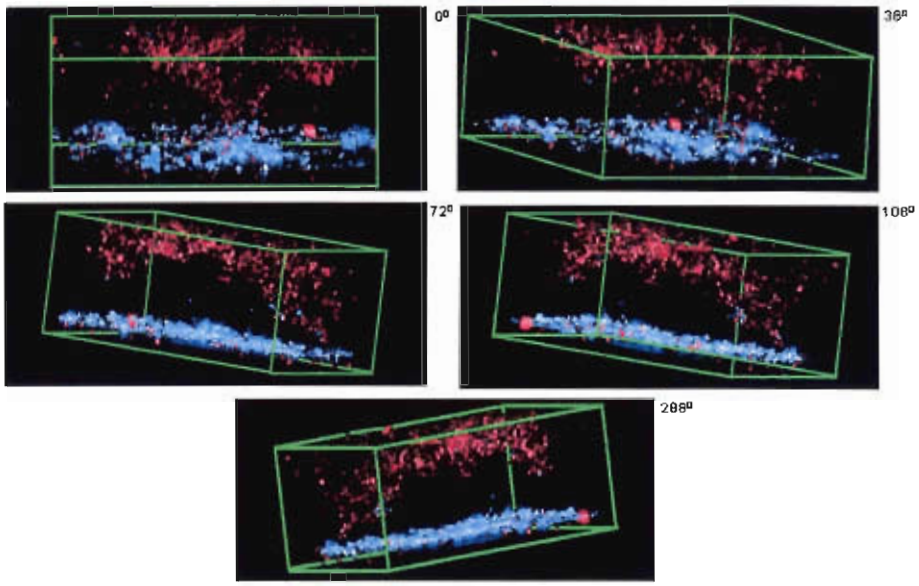

Figure 37. Five perspective views of a 48-hour old monoculture biofilm of *Mycobacterium* strain BT12-100 reconstructed in 3D after introduction of fluorescent, amidine beads, 0.5 µm. Red objects = individual bacteria stained with PI. Blue material = fluorescent beads.

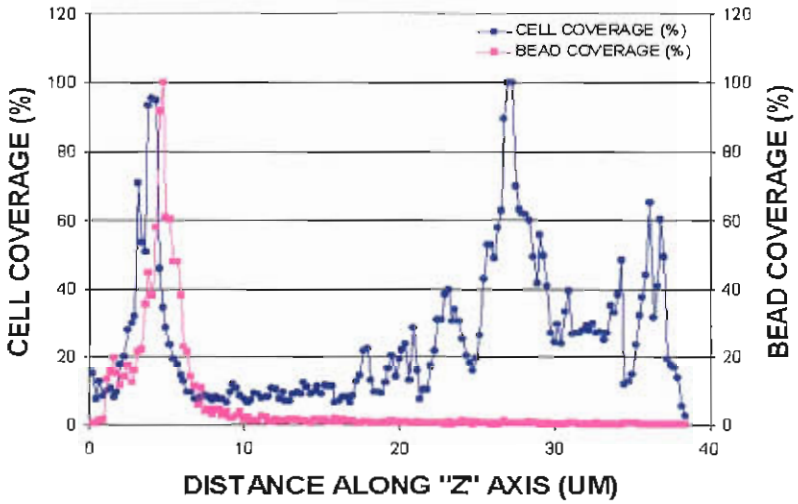

Figure 38. Distribution of bacterial cells and fluorescent beads along the 'z' axis of the total volume of the biofilm depicted in Fig. 37.

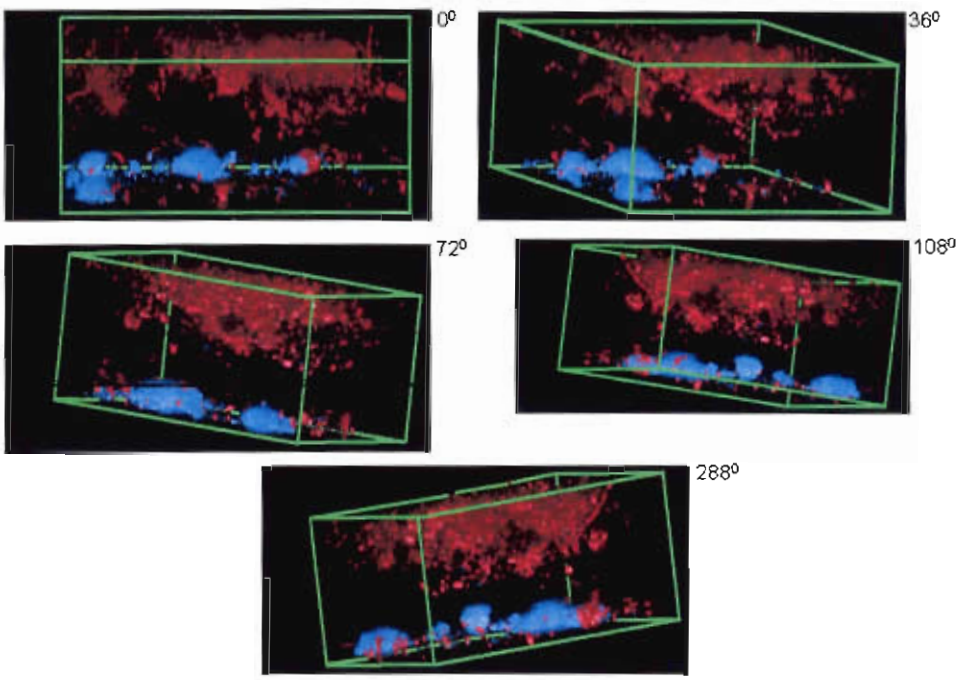

Figure 39. Five perspective views of a 48-hour old monoculture biofilm of *Mycobacterium* strain BT12-100 reconstructed in 3D after introduction of fluorescent, amidine beads, 0.5 µm. Red objects = individual bacteria stained with PI. Blue material = fluorescent beads.

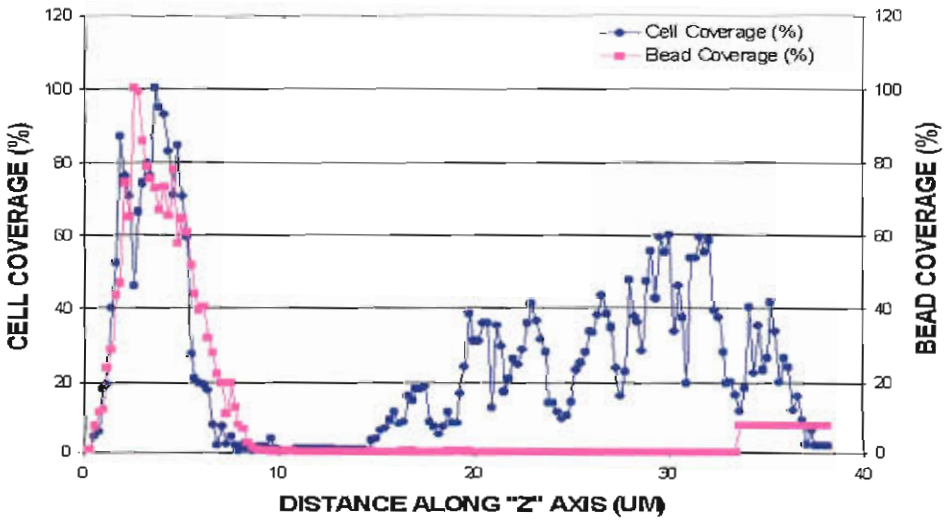

Figure 40. Distribution of bacterial cells and fluorescent beads along the 'z' axis of the total volume of the biofilm depicted in Fig. 39.

In summary, bacterial distribution in both natural biofilms and *Mycobacterium* biofilms (Figs. 28-36) seems to follow the same pattern of arrangement away from the coverglass surface and the top of the biofilm volume. The exopolymer distribution was, however, evenly distributed in all cases but one (Figs. 32 and 33). We can probably conclude that distribution of cells and exopolymer in a natural biofilm is heterogenous, even when formed on the same type of membrane surface.

Detachment Experiments. The MFC was employed in this study to determine how early membrane biofilm structure might be altered by treatment with various chemical agents. It was a goal of this study to identify antibiofouling chemical agents that might be used to improve long-term membrane performance by reducing the duration and/or frequency of membrane cleaning cycles. The compounds tested included (1) the anionic detergents dodecylbenzenesulfonic acid (DBSA), sodium dodecyl sulfate (SDS), and zosteric acid (an anionic natural organic product) (2) the amphoteric alkylsulfonic-ammonio surfactant biocides Zwittergent 3-16, Zwittergent 3-12, and Zwittergent 3-08, (3) the neutral detergents polyethyleneoxide (Triton X100) and (4) chloramine. Each compound was tested separately for its effect on biofilm structure by introducing it into the MFC influent and digitally recording the visual appearance of the biofilm within a selected region of interest over time.

Data presented in Fig. 41 indicate that the anionic surfactant DBSA at a concentration of 0.1 wt% resulted in rapid detachment of *Mycobacterium* strain BT2-4 cells from a 48-hr old MFC biofilm formed on CA-coated coverglass. There was a lag phase of approximately 6 minutes from the time DBSA was introduced until the time initial detachment was observed. This lag period was due to the time required for transport of the DBSA from the point of in-line injection to the interior of the MFC. Thus, cellular response to the DBSA was almost immediate. The kinetics of bacterial detachment were biphasic, i.e., an initial brief rapid phase of cellular detachment was followed by a much slower rate of detachment (See Figs. 41 and 42). As DBSA began to enter the MFC, the majority of attached mycobacteria immediately responded by first undergoing

partial detachment and forming an unstable association with the CA polymer surface. This unstable association was indicated by the abrupt initiation of Brownian motion by previously quiescent immobilized cells. Cells undergoing Brownian motion often precessed about an attachment point as if they were tethered to the CA surface by an invisible strand of polymer or other highly flexible extracellular appendage (e.g., fimbria) (Fig. 43). Brownian motion continued until the cell detached a few seconds later and was transported out of the MFC in the bulk flow. The position of two cells were tracked during DBSA treatment by determining the coordinates of their centroids as a function of time (Fig. 44). Relative motion of the cells was determined by expressing the sum of the X and Y displacement (delta X+Y) of the centroids of each cell as a function of time (Fig. 45). Cell #1 showed little motion during DBSA treatment. Cell #2 exhibited a large displacement, then completely detached after 16 minutes, while cell #1 remained attached to the CA membrane.

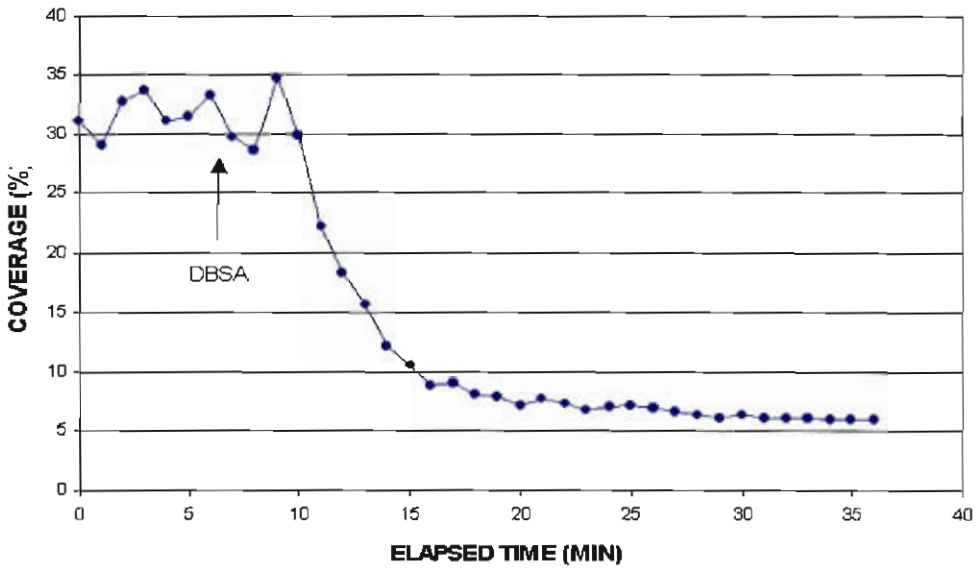

Figure 41. Effect of DBSA on detachment of *Mycobacterium* cells. Note biphasic detachment kinetics (initial rapid detachment phase followed by a slower rate of detachment). About 20% of cells remained unstably attached to membrane surface following detergent treatment. Image analysis software was used to quantify the number of bacteria per field in the Nomarski DIC images.

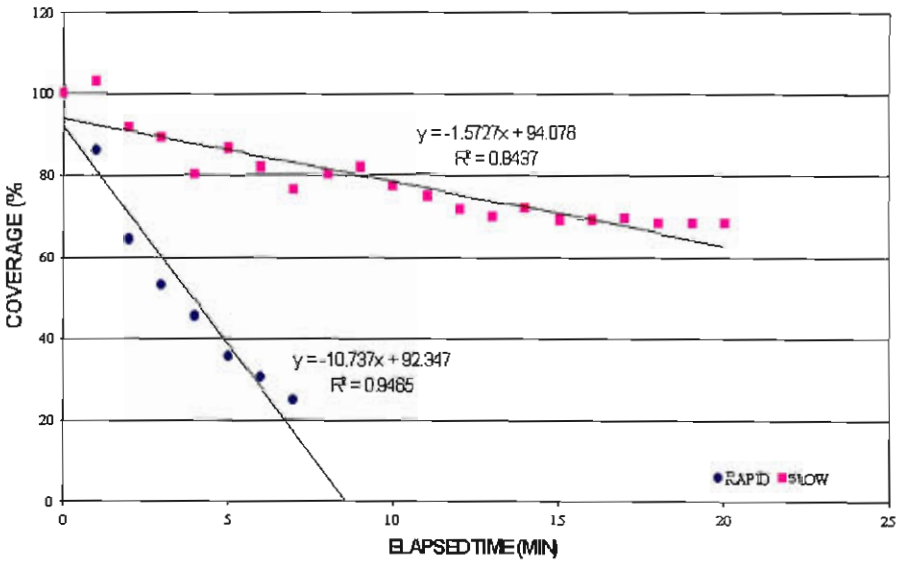

Figure 42. The kinetics of bacterial detachment were biphasic: an initial brief rapid phase of cellular detachment (m=-10.7 min^{-1}) was followed by a much slower but prolonged period of cellular detachment (m=-1.6 min^{-1}). The initial rate of rapid cell detachment was about 7-fold greater than the rate of slow cell detachment for this concentration of DBSA.

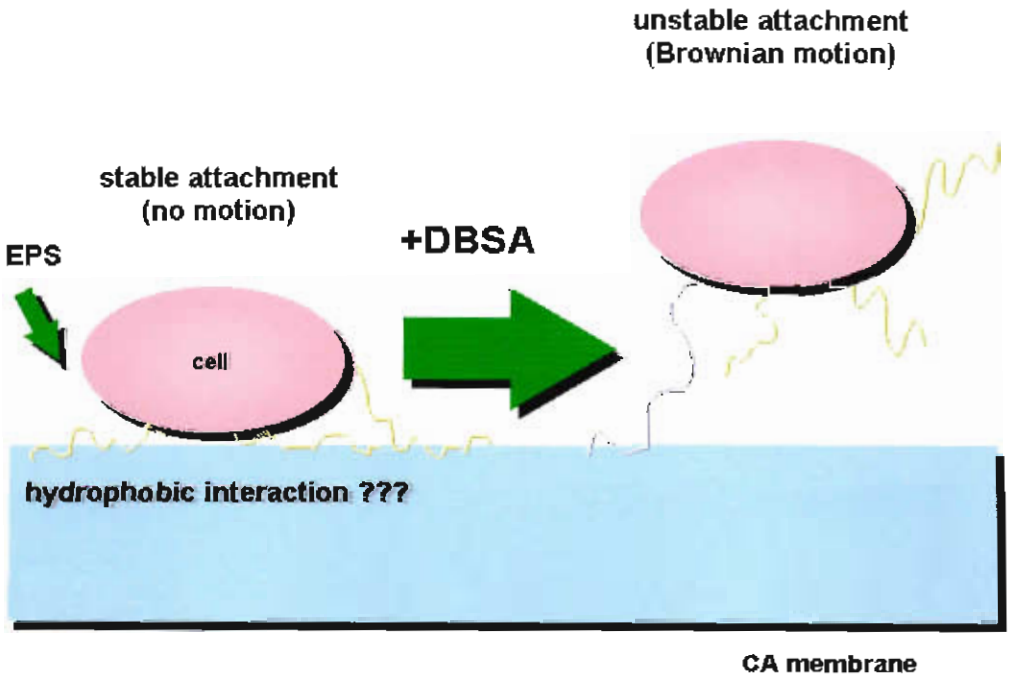

Figure 43. Diagram illustrating transition from stable to unstable attachment of bacterial cell in response to detergent treatment. Unstable attachment may be mediated by EPS material.

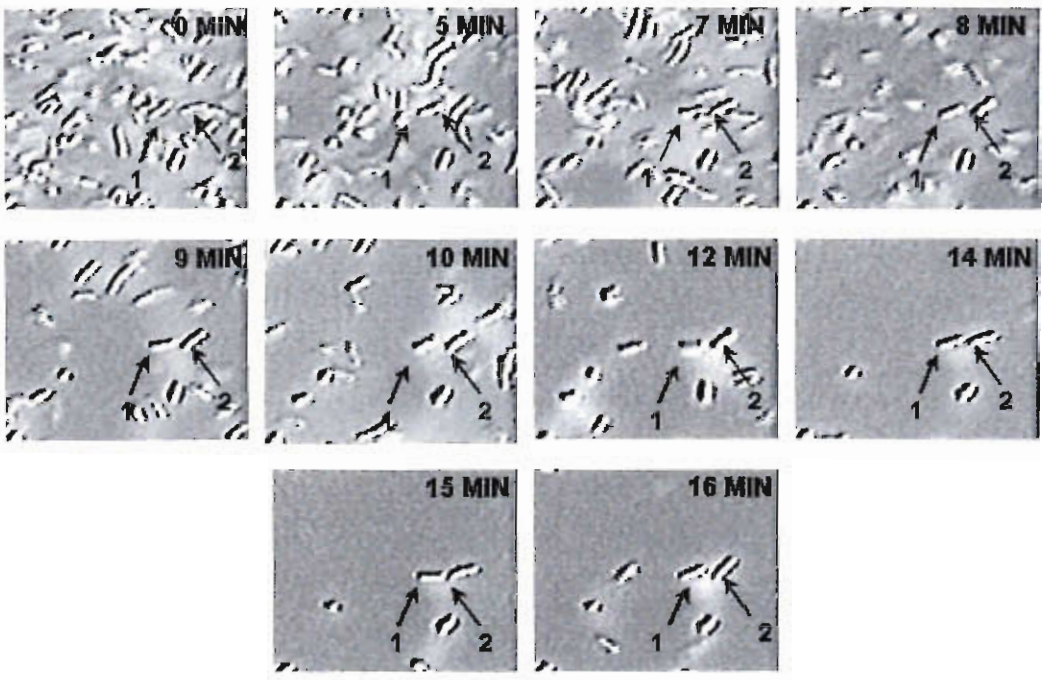

Figure 44. Series of Nomarski images showing cells undergoing Brownian motion.

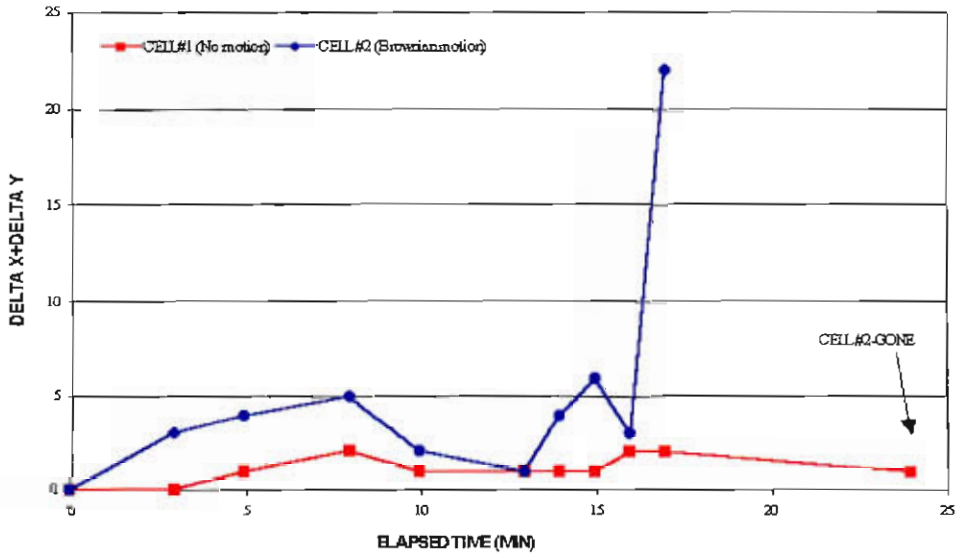

Figure 45. Quantitative analysis of the movement and detachment of one cell (cell #2) compared to an attached cell (cell #1).

Interestingly, not all biofilm cells underwent complete detachment in response to the DBSA treatment. The DBSA typically resulted in about 80-85% loss of attached biofilm bacteria. The remaining attached bacteria continued to exhibit Brownian motion but failed to detach even after prolonged exposure to the DBSA (e.g., 24 hours). Thus, at least two distinct cell populations were observed within this axenic (*Mycobacterium* species) biofilm, one susceptible to rapid and complete removal by 0.1 wt% DBSA, the other resistant to cleaning.

The data presented in Figures 46 and 47 indicate that DBSA was effective at removing early (48-hr) biofilm cells at a concentration of 0.05 wt% but not at 0.01 wt%. Removal kinetics at 0.05 wt% was similar to those previously observed at 0.1 wt%. Attached biofilm cells treated with 0.01 wt% DBSA remained susceptible to removal by subsequent treatment with 0.1 wt% DBSA (Figure 47).

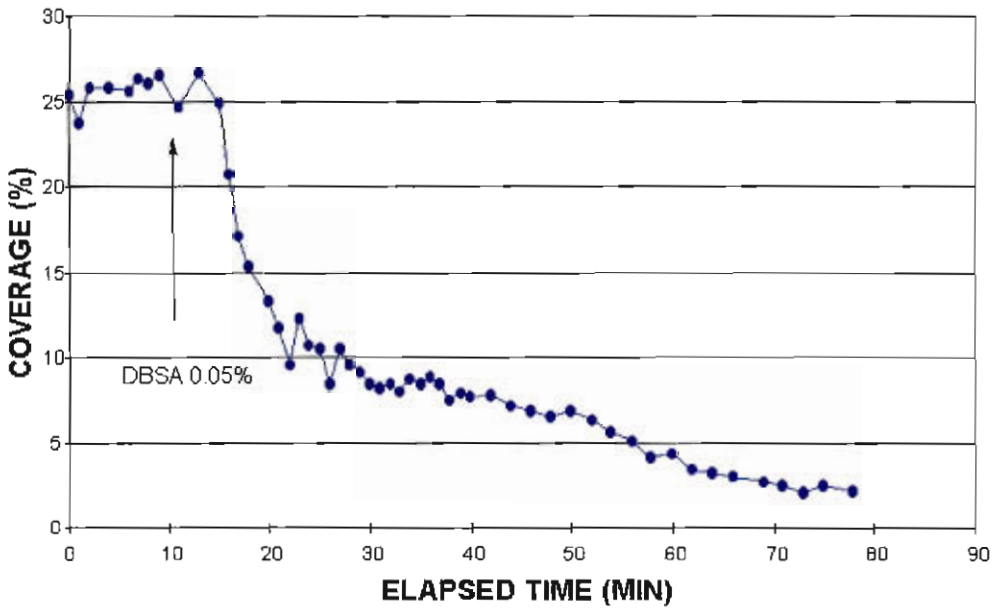

Figure 46. Effect of DBSA (0.05 wt%) on detachment of *Mycobacterium* cells from a biofilm formed on a CA-coated coverglass.

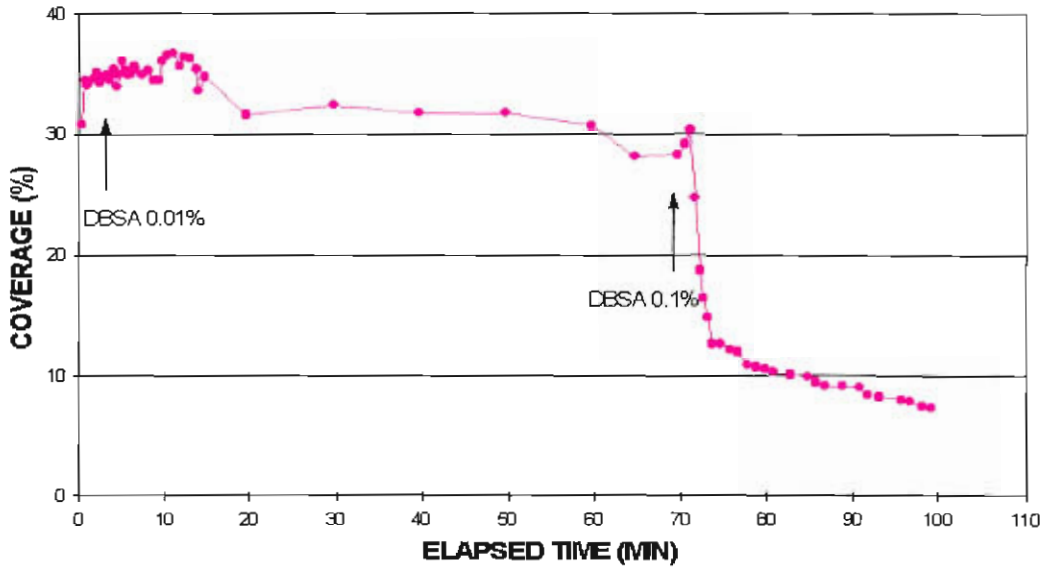

Figure 47. Effect of DBSA (0.01 wt%) on detachment of Mycobacterium cells from a biofilm formed on CA-coated coverglass.

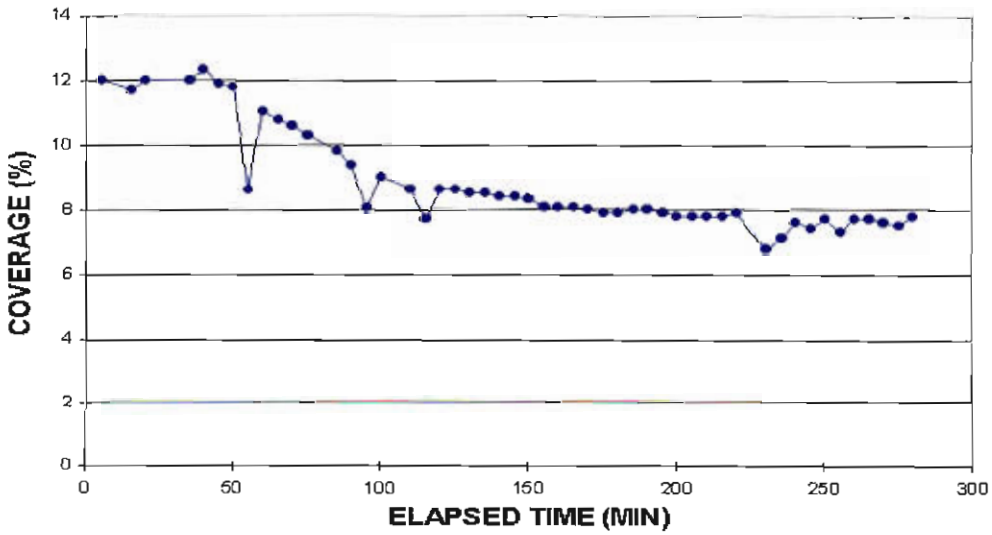

Figure 48. Effect of DBSA (0.1 wt%) on a native biofilm grown on the surface of a CA-coated coverglass.

Exposure of a native biofilm pregrown on the surface of a CA-coated coverglass to DBSA (0.1 wt%) did result in partial detachment of the biofilm (~30% biofilm removal, Fig. 48) but not the extent observed with the axenic *Mycobacterium* biofilms.

In order to more accurately establish the concentration at which DBSA promoted cellular detachment from CA membrane, MFC experiments were performed in which the amount of detergent was varied continuously over a concentration gradient from 0.00-0.16 wt%. As shown in Fig. 49, biofilm cells first began to detach when the DBSA concentration reached approximately 0.05 wt%, a result consistent with previous observations. Increasing the DBSA concentration above this amount did not appear to further enhance cell detachment kinetics. Moreover, as before, some 20% of the original sessile polulation of *Mycobacteria* remained attached to the CA membrane surface even at the highest DBSA concentration. The remaining cells were evidently resistant to the effects of this detergent but exhibited vigorous Brownian motion about an attachment (tether) point, suggesting weakening of attachment.

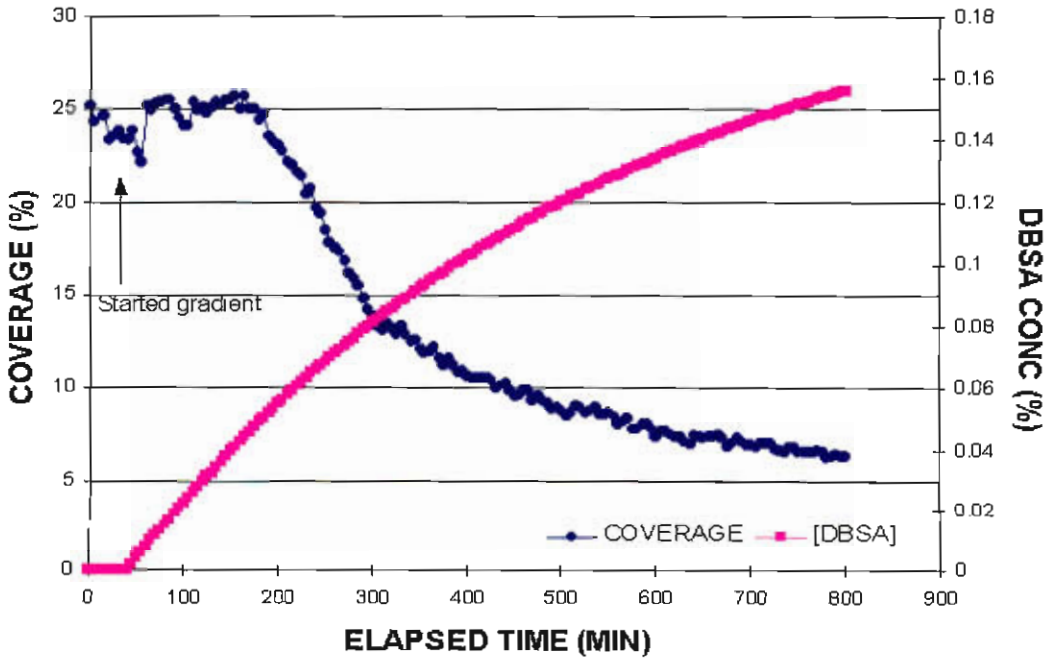

Figure 49. Effect of a DBSA concentration gradient (0 - 1.6 wt%) on detachment of *Mycobacterium* cells from a biofilm formed on a CA-coated coverglass.

The results of a similarly performed concentration gradient experiment indicated that the neutral polyethylene oxide detergent Triton-X100 began to exert a cell detachment effect at a concentration of 0.05 wt% (Fig. 50). However, the detachment effect of Triton-X100 was substantially less than that of anionic DBSA. In addition, a considerably larger portion of the sessile biofilm population (about 60%) remained attach to the CA-coated coverglass following detergent treatment.

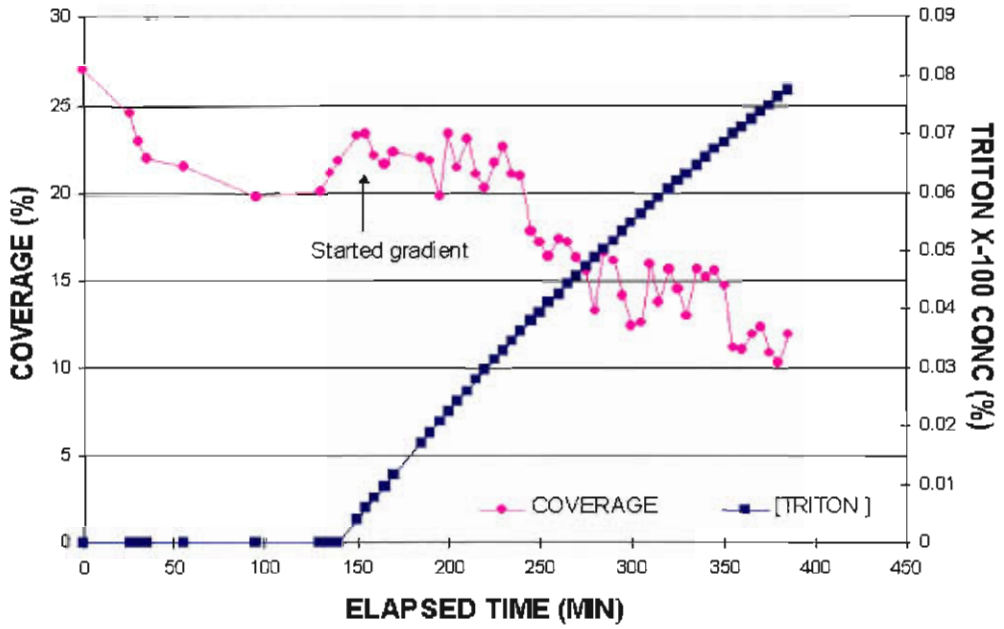

Figure 50. Effect of a Triton X-100 concentration gradient (0 – 0.08 wt%) on detachment of *Mycobacterium* from a biofilm formed on a CA-coated coverglass.

The amphoteric alkylsulfonic-ammonio surfactant compound Zwittergent 3-08 was also found to stimulate mycobacterial detachment from nascent 2-day old CA-coated membrane biofilms (Fig. 51). The kinetics of cell detachment by 0.1 wt% Zwittergent 3-08 were notably slower than that of DBSA but greater than Triton-X100. Like Triton-X100, a large proportion of the sessile biofilm community was evidently resistant to the effects of Zwittergent 3-08 and remained attached following treatment. The kinetics of cell detachment by Zwittergent 3-08 were biphasic like those of DBSA, but cell

detachment during the slow phase (m=-.05 min $^{-1}$) was greater than that observed during the slow detachment phase of DBSA (Fig. 52).

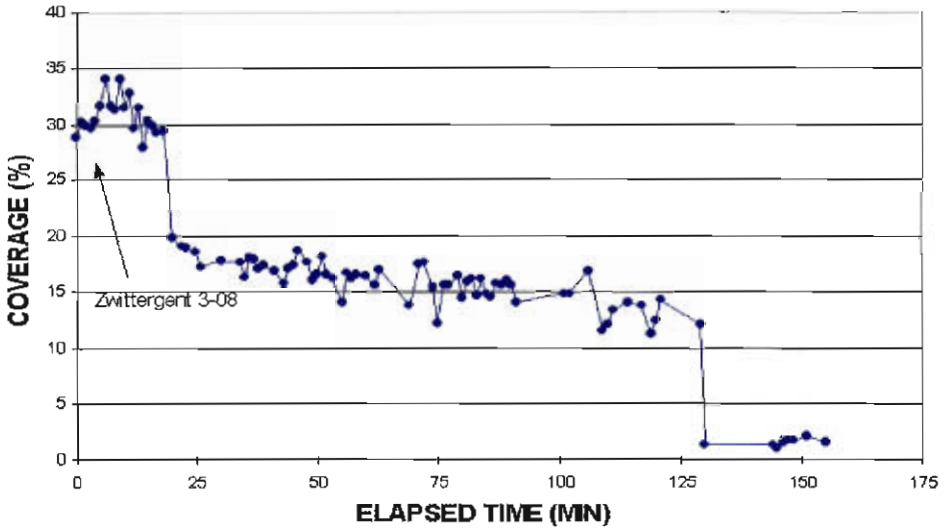

Figure 51. Effect of Zwittergent 3-08 (0.1 wt%) on detachment of *Mycobacterium* cells from a biofilm formed on a CA-coated coverglass.

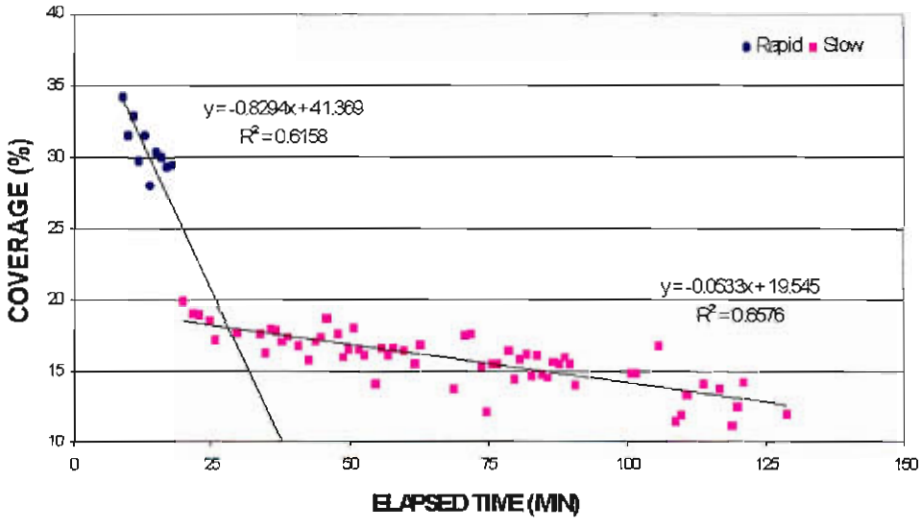

Figure 52. The kinetics of bacterial detachment of Zwittergent 3-08 were biphasic, with cell detachment during slow phase (m=-0.05 min $^{-1}$) being greater than that observed during slow phase of DBSA.

The compound Zwittegent 3-16 possesses an identical molecular structure to that of Zwittergent 3-08 except that the hydrophobic alkyl group is C16 instead of C8. Despite strong molecular similarity, Zwittergent 3-16 was completely ineffective at promoting cellular detachment at concentrations of up to 0.1 wt% . In addition, biofilm cells first treated with Zwittergent 3-16 acquired total resistance to removal by 0.1 wt% DBSA (Fig. 53). The basis for this acquired resistance to DBSA removal is unknown at this time, but could possibly be related to the amphoteric nature of the Zwittergent compounds.

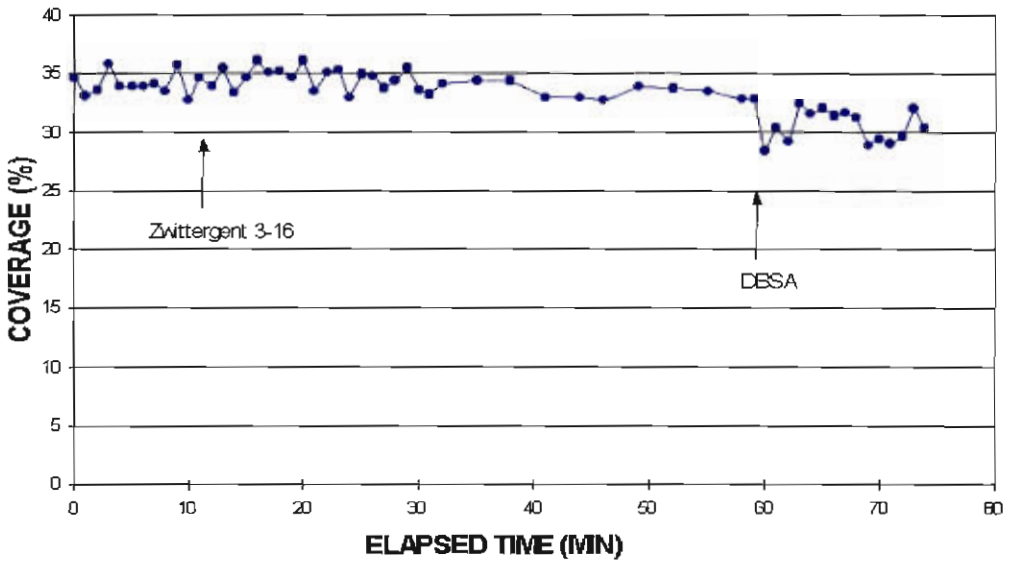

Figure 53. Effect of Zwittergent 3-16 (0.1 wt%) on detachment of *Mycobacterium* cells from a biofilm formed on a CA-coated coverglass.

The addition of the detergent sodium dodecyl sulfate (SDS) resulted in partial detachment of the *Mycobacterium* strain BT12-100 biofilms. Moreover, in this case, the whole biofilm partially detached from the surface as a sheet; the cells appeared to be embedded in a gel-like matrix that exhibited movement with variations in MFC flow, but never completely detached from the surface. The reason for the apparent loss of cells in this figure is that cells raised up out of the objective focal plane during "swelling" of the gel (Fig. 54).

The compound Zwittegent 3-16 possesses an identical molecular structure to that of Zwittergent 3-08 except that the hydrophobic alkyl group is C16 instead of C8. Despite strong molecular similarity, Zwittergent 3-16 was completely ineffective at promoting cellular detachment at concentrations of up to 0.1 wt% . In addition, biofilm cells first treated with Zwittergent 3-16 acquired total resistance to removal by 0.1 wt% DBSA (Fig. 53). The basis for this acquired resistance to DBSA removal is unknown at this time, but could possibly be related to the amphoteric nature of the Zwittergent compounds.

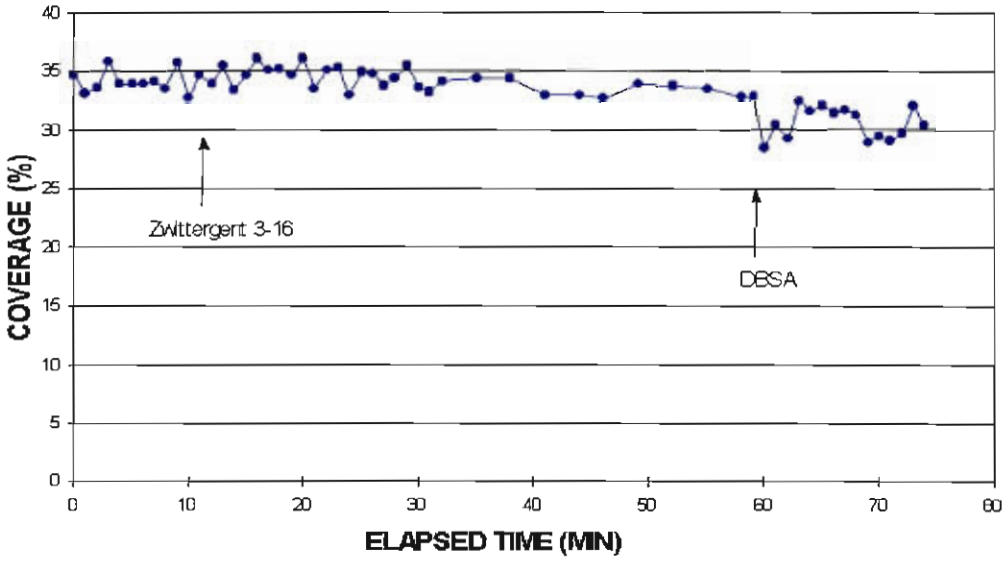

Figure 53. Effect of Zwittergent 3-16 (0.1 wt%) on detachment of *Mycobacterium* cells from a biofilm formed on a CA-coated coverglass.

The addition of the detergent sodium dodecyl sulfate (SDS) resulted in partial detachment of the *Mycobacterium* strain BT12-100 biofilms. Moreover, in this case, the whole biofilm partially detached from the surface as a sheet; the cells appeared to be embedded in a gel-like matrix that exhibited movement with variations in MFC flow, but never completely detached from the surface. The reason for the apparent loss of cells in this figure is that cells raised up out of the objective focal plane during "swelling" of the gel (Fig. 54).

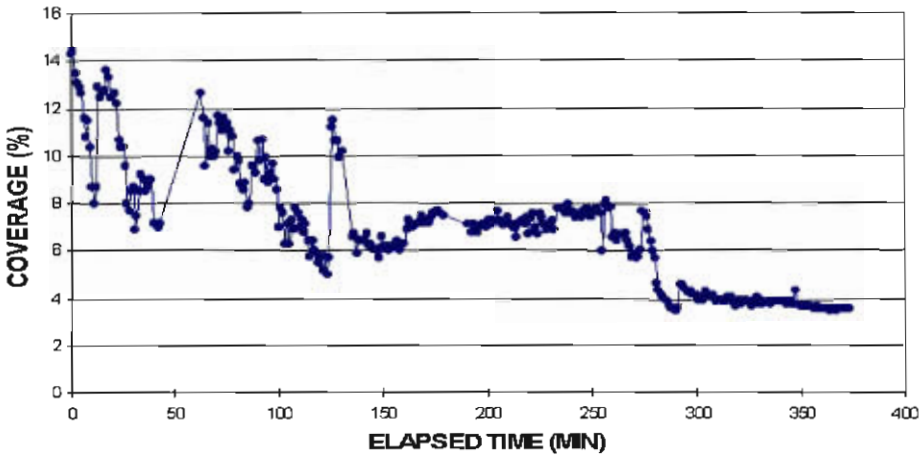

Figure 54. Effect of SDS (0.1 wt%) on detachment of *Mycobacterium* cells from a biofilm formed on a CA-coated coverglass.

Zosteric acid, an anionic organic (plant) product, was tested since it is known to impede biofilm formation in sea water. It had no effect on detachment of BT12-100 biofilm or on preventing attachment of these cells at up to 0.09 wt%. Differences in ionic strength between sea water and the MFC medium might be the explanation for these results (Fig. 55).

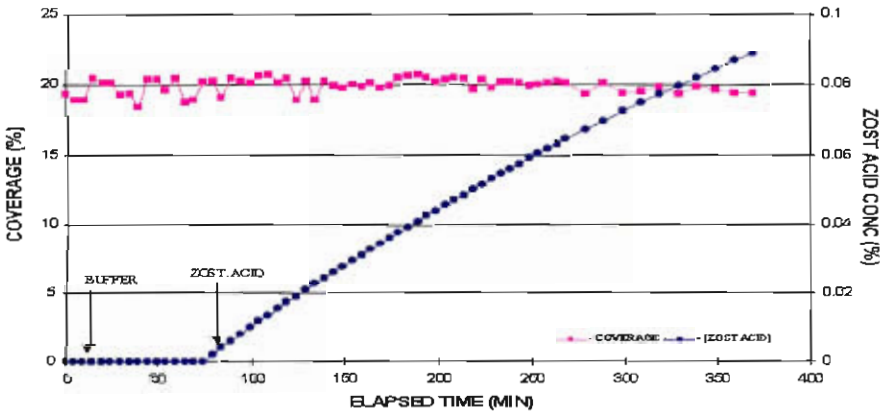

Figure 55. Effect of a Zosteric Acid concentration gradient (0 – 0.09 wt%) on detachment of *Mycobacterium* cells from a biofilm formed on a CA-coated coverglass.

Chloramine was also tested for its ability to detach biofilms of BT12-100 cells. It had no effect when using concentrations of 100-1000 ppm (Fig. 56). However, cell attachment was actually promoted when the CA-coated surface was pre-treated with chloramines, resulting in 57% more attached cells than in an untreated control (Fig. 57). The difference in rates of attachments can be observed on Fig. 58, where a higher rate of attachment was seen on the surface exposed to chloramine ($m=0.49\ min^{-1}$) as opposed to the untreated control ($m=0.14\ min^{-1}$). Chloramine seems to increase the "stickiness" of CA to BT12-100 cells, posibly by increase in charge or maybe oxidation effects.

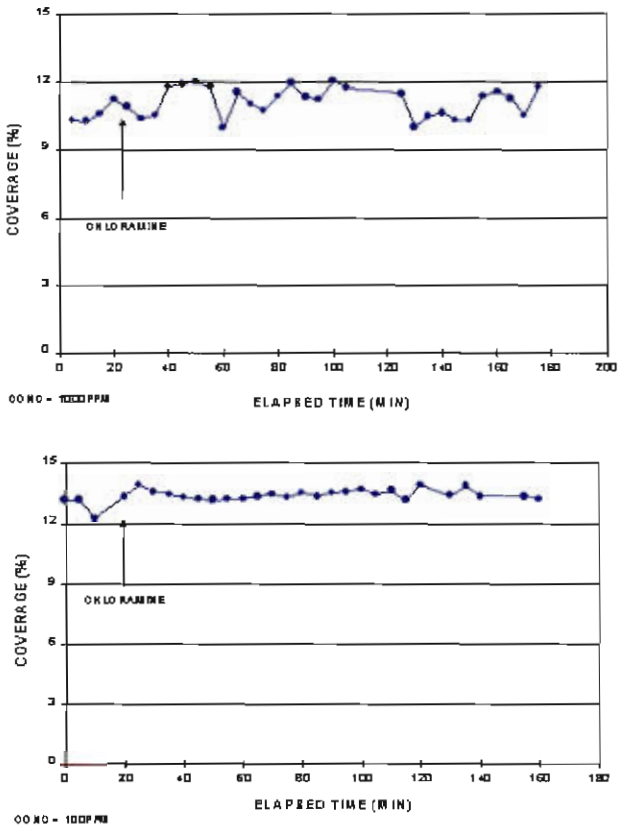

Figure 56. Effect of chloramine (100 and 1000 ppm) on detachment of *Mycobacterium* cells from a biofilm formed on a CA-coated coverglass.

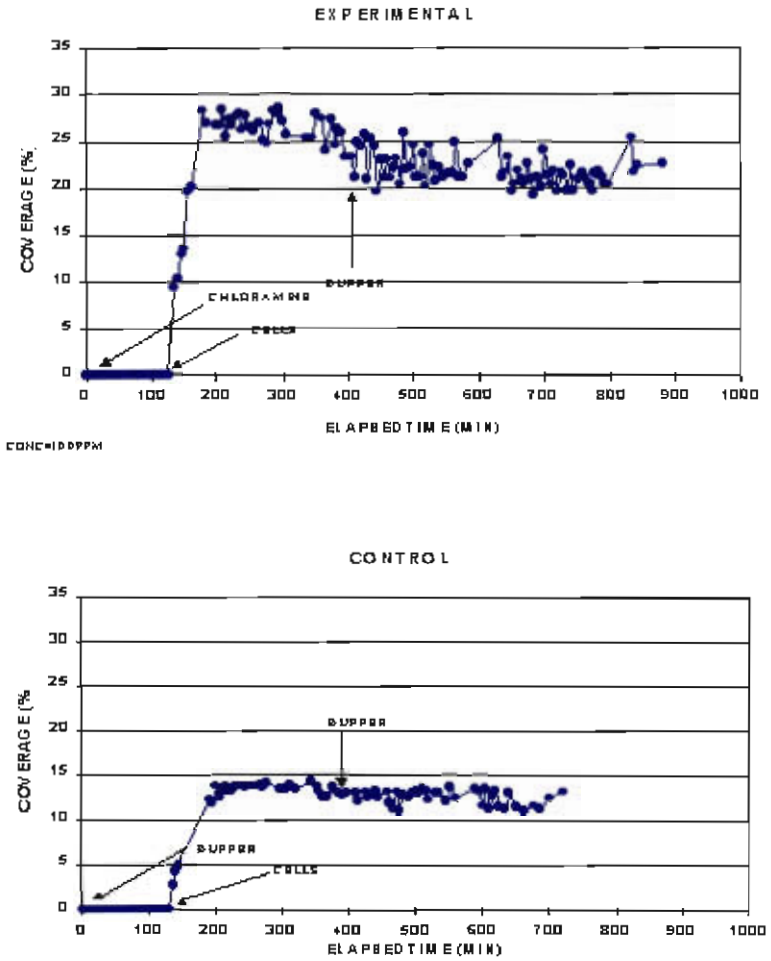

Figure 57. Effect of chloramine (100 ppm) on attachment of *Mycobacterium* cells to a CA-coated coverglass. CA surface was pre-treated with chloramine resulting in faster binding kinetics (m=0.49 min^{-1}) and greater binding capacity (57% increase after chloramine treatment).

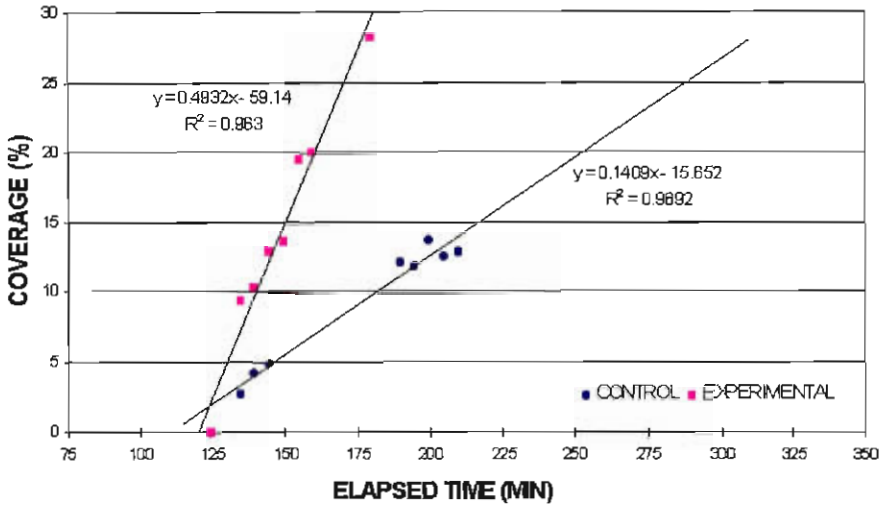

Figure 58. The kinetics of bacterial attachment of chloramine showed a higher rate of attachment on the surface exposed to chloramine ($m=0.49\ min^{-1}$) as opposed to the untreated control ($m=0.14\ min^{-1}$).

DISCUSSION

Microscope Flow Cell (MFC) Design. The pioneering work by Caldwell and colleagues in the late 1980s and early 1990s (13) using flow cells and confocal microscopy to observe fully hydrated biofilms at high resolution led to a shift in our perception of the structure of bacterial biofilms from that of a homogenous layer of cells in a slime matrix to a much more heterogenous and complex arrangement. MFCs of various design configurations have since been developed by others (16, 22, 24).

The MFC may be used to grow and observe axenic or native mixed-species biofilms under controlled physicochemical and hydrodynamic conditions, or it may be placed in line in an actual membrane facility to monitor biofilm formation kinetics on designated feedwater types. MFCs may be used to explore and identify (at the microscopic scale) physical or chemical conditions which disrupt biofilms (e.g., candidate chemical cleaning agents) or that interfere with or otherwise influence biofilm growth kinetics (e.g., biocides). The MFC should be sufficiently flexible in design to accommodate different flow channel geometries (e.g., channel shape and dimensions). Poor MFC design or machining invariably results in flow cells that leak or that are too cumbersome or time consuming to use on a routine basis. Well-designed thermo-regulated MFCs meeting the above criteria are commercially available (e.g., Bioptecs, Inc., Butler, PA, USA). The development and implementation of a microscope flow cell (MFC) was one of the most critical components of this study, since it allowed the direct visualization and quantification of attached membrane biofilm cells under dynamic flow conditions, i.e., during treatment with selected chemical anti-biofouling agents.

The calculated flow velocities that attached bacteria might experience in the MFC were generally lower than those in an actual RO membrane module. However, recent computer modeling studies have revealed that flow in an actual membrane module is highly variable depending on the position of the attached cells relative to the module feed channel spacer material (R.L. Riley, Separation Systems, Inc., San Diego, CA, personal communication). Indeed, large areas of the membrane surface (especially in

the vicinity of the flow spacer) experience flows comparable to those in the MFC. Thus, cell attachment and biofilm growth rate data obtained using the MFC are valid for those areas of actual membrane systems where flow velocities are low (e.g., proximal to the Vexar spacer). Furthermore, use of generally lower flow velocities and shear forces in the MFC provide a more conservative experimental approach, since cell detachment or biofilm disruption observed at the lower flow rates of the MFC could then be expected to also occur at the considerably higher flow rates in actual membrane modules.

An important distinction between the MFC and an actual separation membrane system is that there is no pressure-driven water or solute transport in the MFC, although this force may be minor compared to the hydraulic shear forces. Thus, biofilm formation results exclusively from (i) initial microbial adhesion to the membrane surface as determined by the inherent affinity of bacterial cells for the synthetic polymer membrane surface, and (ii) growth of attached cells at the expense of feedwater nutrients. There is no opportunity for hydraulically-mediated 'filtration' of bacteria onto the membrane surface in the MFC. Thus, biofilm formation under MFC operating conditions might be expected to be slower than that in an actual RO membrane system. Despite this limitation, the MFC has proven extremely useful for rapidly screening conditions that impede initial bacterial adhesion to selected polymer membrane materials or that disrupt existing biofilms.

Membrane Surface Charge Distribution. Hydrated polymeric membranes can have electrically charged surfaces, dependent on the chemical properties of the membrane and the chemistry of the solution (6). Cellulose acetate and composite polyamide membranes acquire a negative surface charge through adsorption of anions from solution (6). The net negative surface charge of CA membrane has been demonstrated in earlier studies (5, 6) using direct base titrations and streaming potential measurements, but no information about charge distribution was provided in those studies. The observations on membrane surface charge distribution in this study strongly suggest that the normal CA membrane surface possesses a net negative surface charge independent of pH, and that this charge is distributed in a patchy fashion

not unlike bacterial attachment itself. These results correspond with those reported by Elimelech et.al. (1994) (6), where cellulose acetate and composite polyamide membranes were shown to remain negatively charged at all pH values greater than 3.5. The PLM binding data from this study suggest the possibility that bacterial adhesion might respond to the uneven membrane surface charge distribution during initial cell attachment.

Biofilm Architecture. An important objective of this study was to explore the submicron architecture of membrane biofilms in order to identify unusual or unique structural features that might provide novel avenues for alternative chemical treatment strategies. In order to achieve this, native multi-species membrane biofilms and mono-culture biofilms were examined under conditions, which, as closely as possible, resemble "in situ" conditions. Under natural conditions, true monospecies biofilms are comparatively rare and in most natural and industrial environments, biofilms are typically complex communities. Diversity in microbial communities lead to a variety of complex relationships involving interspecies and intraspecies interactions (22).

Several generalizations may be made regarding the structure of the natural 5-8 month old multispecies cellulose acetate (CA) and polyamide (PA) membrane biofilms from WF21. The natural multi-species membrane biofilms consisted of cells that were unevenly distributed, with areas of dense cell population separated by sparsely populated regions. This heterogeneity was consistent from biofilm to biofilm. 'Tunnels' or 'open channels' were commonly visible in 3-D reconstructions of the biofilms. The overall thickness of the biofilms varied from 5-70 microns. The same type of characteristics were found in biofilms of a mono-culture of *Mycobacterium*, strain BT12-100. These results are consistent with reports of measurements of thickness variability between biofilms of two different types of bacteria grown in identical reactors at the same operating conditions. In this case, biofilm structure varies from uniformly thin and thick (*P. aeruginosa*) to highly variable and patchy (*K. pneumoniae*), (18). Significant microscale structural heterogeneity occurs in biofilms, and species composition can be an important determinant of biofilm structure.

The biofilms studied by Lawrence et. al., 1990 (13) using CSLM and viable, fluorescent-negative staining technique were highly hydrated, open structures composed of 73-98% non-cellular material. This is largely consistent with our observations of CA and PA biofilms. Biofilms studied by CSLM are widely reported to be heterogenous and consist of micro-colonies or cell clusters (aggregates of microbial cells in an extracellular polysaccharide matrix) separated by interstitial voids and channels (4, 15, 16), and it has been discovered that water could flow through channels (25). These observations are also in agreement with our results. Furthermore, membrane type did not significantly affect 3D structures. Likewise, biofilms formed on CA membranes at WF21 were essentially indistinguishable morphologically from those that formed on PA membranes.

Presence of extacellular polymeric substances (EPS) was confirmed by observation of a diffused background of PI stain in the void spaces. EPS in these regions could provide physically integrity to the biofilm matrix and slow the diffusion-mediated transport of water and solutes across the biofilm. It is currently unclear whether it is the EPS material itself, the dispersed cells, or some combination of the two that are responsible for water flux decline in membrane systems. Moreover, the nature of the EPS (its chemical composition and physical properties) could radically alter its permeation properties for water and solutes. Stewart et. al., 1995 (24) found that staining of frozen sections of a biofilm with ethidium bromide and calcofluor white indicated that nucleic acid and polysaccharides are distributed differently. The ethidium bromide-stained region was contained within the larger region of calcofluor staining; thus, some cell-free areas actually were filled with EPS. This is also the case with many of the membrane biofilms examined in this study.

Muti-species MFC biofilms grown for 48 hours on CA-coated coverglasses, fed with actual secondary effluent from WF21 were similar in appearance and overall thickness to the 5-8 month old native membrane biofilms described above. The distribution of individual cells comprising the 48-hr old biofilms was also uneven and patchy resulting

in spatial heterogeneity. As in the older native RO membrane biofilms described above, EPS materials appeared to fill some of the channels and void spaces between individual cells or group of cells.

Dual staining of the biofilm (cells and exopolymer) provided us with both qualitative and quantitative information about the sub-micron structure of axenic laboratory-grown and natural multi-species bofilms. The distribution of bacterial cells and extracellular polysaccharides along the 'Z' axis of the total volume of the biofilm can be followed and compared to other biofilms. In natural biofilms, this distribution varied from specimen to specimen. The presence of EPS seemed to be evenly distributed throughout the biofilm or, in one case, was denser closer to the membrane surface, where density of the cells was also higher. Cell density was typically greatest around the middle of the biofilm volume, in most cases. Channeling near the membrane surface typically results in a sparser cell population, and hydrodynamic shearing in the upper layers of the biofilm may reduce the cell population in this region, thus explaining this observation.

The fact that fluorescent beads penetrated mostly along the CA-coated surface suggests that there are probably channels or tunnels close to the membrane surface in some of these biofilms, and that laminar flow may transport materials beneath the cell layers of the biofilm in these channels.

The distribution of bacterial cells and extracellular polysaccharides in mono-culture biofilms of *Mycobacterium*, strain BT12-100 was somewhat different than the multi-species biofilms. The cells were more evenly distributed throughout the biofilm than the cells in multi-species examples, and the cell density was also found to be higher in the mono-species biofilms. There were areas where the cells grew in a mushroom-like type of arrangement, with a monolayer of cells more strongly attached to the surface supporting the clusters of cells above the surface, growing towards the top of the biofilm. The mushroom-like structures resulted in "channels" forming near the surface. Once a biofilm was formed, planktonic cells continued adhering to the attached cells. This phenomenon has been reported by Hall-Stoodley et. al., 1999 (9) when working

with *Mycobacterium fortuitum* and *Mycobacterium chelonae* biofilms formed on silastic rubber and high density polyethylene (HDPE) coupons. The growth of these organisms within biofilms should not be overestimated, since they are able to grow under very low nutrient conditions (in sterile tap-water) (9). Jayaraman et. al., 1998 (11) reported that replenishing the medium caused an increase in the uniformity of the distribution of cells throughout the biofilm of *Pseudomonas fragi* and *Escherichia coli*. The distribution of exopolymeric substances (EPS) was reported from the bottom layer of attached cells across the biofilm volume to the top of the biofilm. In some cases the exopolymer:cell volume ratio is higher near the membrane surface and at the top of the biofilm volume and in other cases it was only higher at the top of the biofilm. Initial exopolymer appearance near the surface could play a role in initial adhesion of bacteria to surfaces by binding across the repulsion barrier and thereby anchoring the cell to the surface (or to other cells) (22). The results from both natural biofilms and mono-species biofilms suggest that these biofilms are very heterogenous in terms of distribution of cells and exopolymer.

Biofilm thickness was another variable to consider. We have observed thicknesses of up to 70 microns in natural occurring membrane biofilms. Biofilm thickness may vary considerably over a given substratum due to morphological features of the biofilm (2) and shear forces.

Effect of Chemicals. The detachment of *Mycobacterium sp.* from biofilms by DBSA treatment was very drastic and almost instantaneous. The existence of two distinct removal kinetics could be due to a proximity threshold effect; at the beginning when the cells are very close to each other and also arranged in clumps, the detachment process occurs faster than when cells are more distant from one another, and scattered along the surface. Biphasic kinetics may also be attributed to two distinct populations in the biofilm, a weakly attached population and a strongly attached population of cells. These observations resemble those made during an investigation regarding biofilm resistance to antimicrobial agents (8). Here, biofilm disinfection was also biphasic and consistent with the existence of an inherently resistant population within the biofilm. Resistance to

biocides is one of the important features of biofilm bacteria (7). For example, hydrogen peroxide (H_2O_2) has been reported to be significantly less effective at killing *Pseudomonas aeruginosa* in biofilms than when the cells were planktonic, suggesting that the biofilm imparts a physiological resistance to H_2O_2. In this study Zwittergent 3-16, zosteric acid and chloramine had no effect on removal of cells from *Mycobacterium* biofilms. Triton X-100 and Zwittergent 3-08 induced cell detachment that was substantially less than that of DBSA. Campbell et. al. (1) reported that more surfactants were effective in impairing cell attachment than in promoting detachment. Chloramine pre-treatment of CA membrane was shown to promote cell attachment. SDS, which resulted in partial detachment of the whole biofilm, may make the biofilm more susceptible to shear forces than other chemical agents.

The relative permeability and role of the biofilm channels in providing access for chemical agents which disrupt membrane biofilm structure is currently unknown. However, this question might be addressed by the use of deconvolution microscopy (DCM) using fluorescent versions of some compounds which have been demonstrated to disrupt biofilm structure.

CONCLUSIONS

- Use of the microscope flow cell (MFC) in combination with deconvolution microscopy (DCM) and image analysis tools provided both qualitative and quantitative information about the sub-micron structure of axenic laboratory-grown and natural multi-species biofilms on cellulose acetate and polyamide membranes.

- Three dimensional structure of intact biofilms was viewed using a unique digital deconvolution microscope (DCM) system combined with 3D reconstruction from stacked digitized optical sections and image analysis tools. Dual staining of the biofilm (cells and exopolymer) permited the mapping of multiple biofilm features and provides both qualitative and quantitative information about the sub-micron structure of axenic laboratory-grown and natural multi-species biofilm. This study showed that: (1) heterogeneity in mono-culture and multiple-species membrane biofilms was consistent, (2) exopolymer and bacterial cell distribution was different from biofilm to biofilm, and (3) membrane type (cellulose acetate or polyamide) did not affect 3D biofilms structure.

- Introduction of chemical agents into the MFC containing a membrane biofilm provided new insights concerning how selected test compounds affect the structure of membrane biofilms. DBSA, Triton X-100 and Zwittergent 3-08 effectively promoted cell detachment of mycobacteria from surfaces of simulated CA membranes in the MFC. SDS led to swelling of the biofilm, while zosteric acid, Zwittergent 3-16 and chloramine had no effect.

- Cellulose acetate and composite polyamide membranes were demonstrated to possess a negative surface charge, independent of pH variations.

REFERENCES

1. Campbell, P., Srinivasan, R., Knoell, T., Phipps, D., Ishida, K., Safarik, J., Cormack, T. and H. Ridgway. 1999. Quantitative structure-activity relationship (QSAR) analysis of surfactants influencing attachment of a *Mycobacterium sp.* to cellulose acetate and aromatic polyamide reverse osmosis membranes. Biotechnol. Bioeng. 64(5):527-544.

2. Christensen, B.E. and W.G. Charaklis. 1990. Physical and Chemical Properties of Biofilms. In: Biofilms. Ed: William G. Charaklis and Kevin C. Marshall, John Wiley & Sons, Inc., New York.

3. DeBeer, D., Stoodley, P., Roe, F. and Z. Lewandowski. 1994. Effects of biofilm structures on oxygen distribution and mass transfer. Biotechnol. Bioeng. 43:1131-1138.

4. DeBeer, D., Stoodley, P. and Z. Lewandowski. 1997. Measurement of local diffusion coefficients in biofilms by mircroinjection and confocal microscopy. Biotechnol. Bioeng. 53:151-158.

5. Demisch, H.-U. and W. Pusch. 1976. Ion exchange capacity of cellulose acetate membranes. J. Electrochem. Soc. 123(3):370-374.

6. Elimelech, M., Chen, W.H., and J.J. Waypa. 1994. Measuring the zeta (electrokinetic) potential of reverse osmosis membranes by a streaming potential analyzer. Desalination. 95:269-286.

7. Foley, I. And P. Gilbert. 1996. Antibiotic resistance of biofilms. Biofouling. 10:331-346.

8. Grobe, K.J. 1999. Investigation of biofilm resistance to antimicrobial agents. Thesis, M.S. Chemical Engineering, The Center for Biofilm Engineering at Montana State University-Bozeman.

9. Hall-Stoodley, L., Keevil, C.W. and H.M. Lappin-Scott. 1999. *Mycobacterium fortuitum* and *Mycobacterium chelonae* biofilm formation under high and low nutrient conditions. J. Appl. Microbiol. Symposium Supplement. 85:60S-69S.

10. Hassett, D.J., Elkins, J.G., Ma, J-F and T.R. McDermott. 1999. *Pseudomonas aeruginosa* biofilm sensitivity to biocides: use of hydrogen peroxide as model antimicrobial agent for examining resistance mechanisms. In: Methods in Enzymology, Vol. 310. Edited by Ron J. Doyle, Academic Press, San Diego, California.

11. Jayaraman, A., Sun, A.K. and T.K. Wood. 1998. Characterization of axenic *Pseudomonas fragi* and *Escherichia coli* biofilms that inhibit corrosion of SAE 1018 steel. J. Appl. Microbiol. 84:485-492.

12. Lawrence, J.R., Korber, D.R., Hoyle, B., Costerton, J.W. and D.E. Caldwell. 1990. Visualization of microbial biofilm architecture using confocal scanning laser microscopy. Abstracts of the 90th Annual Meeting of the American Society for Microbiology, Anaheim, California.

13. Lawrence, J.R., Korber, D.R., Hoyle, B.D., Costerton, J.W. and D.E. Caldwell. 1991. Optical sectioning of microbial biofilms. J. Bacteriol. 173:6558-6567.

14. Massol-Deya, A.A., Whallon, J., Hickey, R.F. and J.M. Tiedje. 1994. Channels structures in aerobic biofilms of fixed-film reactors treating contaminated groundwater. Appl. Environ. Microbiol. 61:769-777.

15. Møller, S., Sternberg, C., Andersen, J.B., Christensen, B.B., Ramos, J.L., Givskov, M. and S. Molin. 1998. In-situ gene expression in mixed-culture biofilms: evidence of metabolic interactions between community members. Appl. Environ. Microbiol. 64(2):721-732.

16. Mueller, R.F., Characklis, W.G., Jones, W.L. and J.T. Sears. 1992. Characterization of initial events in bacterial surface colonization by two Pseudomonas species using image analysis. Biotechnol. Bioeng. 39:1161-1170.Stoodley, P., Boyle, J.D., deBeer, D. and H.M. Lappin-Scott. 1999. Evolving perspectives of biofilm structure. Biofouling. 14(1):75-90.

17. Murdock, J.W. 1978. Mechanics of fluids. In: Mark's Standard Handbook for Mechanical Engineers. 8th Edition. T. Baumeister, E.A. Avallone and T. Baumeister III, eds. pp. 3-33 3-70, McGraw-Hill Book Co., New York & San Francisco.

18. Murga, R., Sterwart, P.S. and D. Daly. 1995. Quantitative analysis of biofilm thickness variability. Biotechnol. Bioeng. 45:503-510.

19. Phipps, D.; G. Rodriguez and H. Ridgway. 1999. Deconvolution Fluorescence Microscopy for Observation and Analysis of Membrane Biofilm Architecture. In Methods in Enzymology, Vol. 310, pp. 178-194. Ron J. Doyle, ed. Academic Press, San Diego, CA, USA.

20. Reasoner, D.J. and E.E. Geldreich. 1985. A new medium for the enumeration and subculture of bacteria from potable water. Appl. Environ. Microbiol. 49:1-7.

21. Shaw, P.J. 1995. Comparison of Wide-Field/Deconvolution and Confocal Microscopy for 3D Imaging, in "Handbook of Biological Confocal Microscopy" (J.B. Pawley, ed.), p.373. Plenum Press, New York.

22. Shotton, D. and N. White. 1989. Confocal scanning microscopy: three dimensional biological imaging. Trends in Biochemical Sciences. 14:435-439.

23. Skillman, L.C., Sutherland, I.W. and M.V. Jones. 1999. The role of exopolysaccharides indual species biofilm development. J. Appl. Microbiol. Symposium supplement. 85:13S-18S.

24. Stewart, P.S., Murga, R., Srinivasan, R. and D. deBeer. 1995. Biofilm structural heterogeneity visualized by three microscopic methods. Wat. Res. 29(8):2006-2009.

25. Stoodley, P., deBeer, D. and Z. Lewandowski. 1994. Liquid flow in biofilm systems. Appl. Environ. Microbiol. 60:2711-2716.

26. Stoodley, P., Boyle, J.D., DeBeer, D. and H.M. Lappin-Scott. 1999. Evolving perspectives of biofilm structure. Biofouling. 14(1):75-90.